Nanoparticle/Metal–Organic Framework Composites for Catalytic Applications: Current Status and Perspective

Wenlong Xiang [1], Yueping Zhang [2], Hongfei Lin [3],* and Chang-jun Liu [1],*

[1] Collaborative Innovation Center of Chemical Science and Engineering, School of Chemical Engineering and Technology, Tianjin University, Tianjin 300072, China; WenlongX@tju.edu.cn

[2] Department of Chemistry, Tianjin University, Tianjin 300350, China; ypzhang@tju.edu.cn

[3] Voiland School of Chemical Engineering and Bioengineering, Washington State University, Pullman, WA 99164, USA

* Correspondence: hongfei.lin@wsu.edu (H.L.); ughg_cjl@yahoo.com (C.-j.L.); Tel.: +1-509-335-1341 (H.L.); +86-022-2740-6490 (C.-j.L.)

Abstract: Nanoparticle/metal–organic frameworks (MOF) based composites have recently attracted significant attention as a new class of catalysts. Such composites possess the unique features of MOFs (including clearly defined crystal structure, high surface area, single site catalyst, special confined nanopore, tunable, and uniform pore structure), but avoid some intrinsic weaknesses (like limited electrical conductivity and lack in the "conventional" catalytically active sites). This review summarizes the developed strategies for the fabrication of nanoparticle/MOF composites for catalyst uses, including the strategy using MOFs as host materials to hold and stabilize the guest nanoparticles, the strategy with subsequent MOF growth/assembly around pre-synthesized nanoparticles and the strategy mixing the precursors of NPs and MOFs together, followed by self-assembly process or post-treatment or post-modification. The applications of nanoparticle/MOF composites for CO oxidation, CO_2 conversion, hydrogen production, organic transformations, and degradation of pollutants have been discussed. Superior catalytic performances in these reactions have been demonstrated. Challenges and future developments are finally addressed.

Keywords: metal–organic frameworks; MOF; nanoparticle; composites; catalyst; photocatalyst
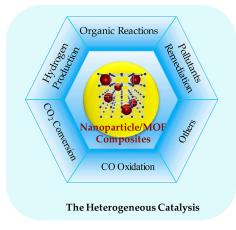
1. Introduction

Metal–organic frameworks (MOFs) are a class of highly porous crystalline materials, which are assembled by the coordination of metal ions with organic ligands [1–4]. Due to the reversibly self-correcting kinetic characteristics that are controlled by the moderate coordination bond energies, MOF materials have exhibited their unique features, such as clearly defined crystal structures, high surface areas, tunable and uniform pore structures, and special confined nanopore microenvironments [5,6]. These features make them promising materials for numerous applications. Nevertheless, a few weaknesses, such as limited electrical conductivity, poor thermal, and chemical stability, prohibit MOFs from exhibiting their full potential for practical applications. Therefore, it is urgently needed to further enhance the functional properties of MOF materials. Recently, the attempts have been made by combining MOFs with various functional materials to produce new functional composites. These MOF based composite materials can integrate the excellent properties and mitigate the shortcomings of the individual components. The synergistic effects of both MOFs and other active components may cause the composites to possess new properties

and unprecedented performance, which are not attainable by the individual parts. Up to now, MOF composites have been successfully fabricated with incorporating various active species, including metal or metal oxides nanoparticles (NPs), carbon materials, polymers, polyoxometalates (POMs), quantum dots (QDs), ionic liquids (ILs), and so on [7–13]. These MOF composites have been widely employed in the areas of gas storage, separation, sensing, biomedicine, protection of bio-macromolecules, and catalysis [14–23].

In term of catalytic application, MOF composites show some superior characteristics because of the unique features of MOFs mentioned above. For example, high porosity with ordered crystalline pores and high surface areas contribute to the uniform dispersion and the high density of catalytic sites, which can improve the catalytic efficiency [5]. The confined pore sizes can limit active species growth and agglomeration, and selectively transport different substrate molecules for size-selective catalysis [24,25]. These superior characteristics have made these composite materials promising in heterogeneous catalysis.

To date, even though MOF composites, as heterogeneous catalysts, are still at a developing stage, a series of catalytic investigations have been reported. It has been demonstrated that MOF composites as heterogeneous catalysts have showed notable catalytic behavior, such as high activity, good stability, and reusability [5,8,12,16–18]. Although some reviews have been published covering some topics on heterogeneous catalysis of MOF composites, this review aims to summarize the recent advances in this hot topic, including CO oxidation, CO_2 conversion, hydrogen production, organic reaction and pollutants remediation, and so on, over nanoparticle/MOF composite based catalysts (Scheme 1).

Scheme 1. Heterogeneous catalysis of nanoparticle/metal–organic frameworks (MOF) composites.

2. General Synthesis of Nanoparticle/MOF Composites

There are three main established approaches for the immobilization of functional molecules or nanoscale objects in MOFs, known as "ship in bottle" approach, "bottle around ship" approach, and one-step synthesis approach.

The "ship in bottle" approach involves the encapsulation of active small molecules components or NPs precursors in the cavities of MOFs, followed by further treatment leading to the desired functional structure (Figure 1a). Various techniques, such as solution infiltration, vapor deposition, and solid grinding have been exploited for introducing the NPs precursors into MOFs [7,26]. It is significantly challenging to precisely control the location, composition, structure, and morphology of incorporated guests when using this synthesis strategy. Zhang et al. [27] summarized the recent progresses in the size and structure control of MOF supported noble metal catalysts. In addition, the possible formation of the precursors and products on the external surface of MOFs needs to be considered. In order to avoid NPs aggregation on the external surface of MOFs, a double-solvent method (DSM) was successfully developed to rationally introduce precursors into MOF pores, followed by further treatment, to produce

NPs@MOF composites [9,28]. The DSM is based on a hydrophilic and hydrophobic solvent, and the large cages with hydrophilic environments and high pore volumes in some MOFs. The quantitative volume (less than the MOF pore volume) of the aqueous precursor solution can be readily incorporated into the pores of MOF, which was suspended in a large amount of low-boiling-point hydrophobic solvent, by capillary force and hydrophilic interactions. By using the DSM combined with the reduction with reducing agents, such as H_2 and $NaBH_4$, metallic NPs including Pt, Pd, Rh, Ni NPs, and AuNi, RuNi, AuCo, and CuCo bimetallic NPs were successfully immobilized inside the pores of MOFs without aggregation on the external surface of the framework [28–33].
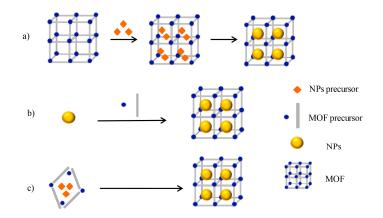

Figure 1. Main approaches for the fabrication of nanoparticle/MOF composites. (**a**) Ship in bottle; (**b**) bottle around ship; and, (**c**) in situ one-step synthesis.

The "bottle around ship" approach, also known as the template synthesis approach, generally involves two steps (Figure 1b). Firstly, the functional molecules or NPs are synthesized individually and often stabilized by capping agents or surfactants. Subsequently, the pre-synthesized nanoscale objects are added into a synthetic solution containing MOF precursors to assemble the MOF. The nanoscale objects do not occupy the pore space of the MOF, but instead are surrounded by grown MOF materials. By using this method, the problems of the aggregation of NPs on the external surface of MOFs are limited, the size, morphology, and structure of entrapped NPs can be easily controlled because they are preformed prior to the assembly of MOF framework [26,34]. However, the introduction of NPs sometimes results in difficulties with the subsequent growth of the MOF because of the high interfacial energy barrier between the two kinds of materials. In addition, the presence of the capping agents (for example, polyvinyl pyrrolidone PVP) might be unfavorable for the complete exposure of active sites, and even alter or degrade the performance of the NPs.

A one-step synthesis approach involves directly mixing the precursors solution of NPs and MOFs together, followed by the simultaneous growth of NPs and MOF, and assembling both of them into a nanostructure (Figure 1c). When compared with the above stepwise approaches, this strategy is straightforward and simple, but it usually needs to balance the rates of the self-nucleation and growth of the NPs and MOFs. In particular, the choice of the functional groups in organic linkers or solvents is vital for trapping the NPs precursors and stabilizing the NPs that were formed in situ and for facilitating the hetero-nucleation of the MOFs on the surface of the NPs [9,35].

The different preparation methods of the catalyst may result in a noticeable difference of catalytic performance. For example, the uniform Pt NPs were successfully supported on or encapsulated inside MOF particles to prepare Pt/UiO-66-NH$_2$ and Pt@UiO-66-NH$_2$ catalysts, through the solution infiltration technique (the "ship in bottle" approach) and "bottle around ship" approach, respectively [36]. The different methods cause a difference in the Pt location relative to the MOF, which leads to a very different photocatalytic activity. The internal Pt NPs in the MOF greatly shortens the path of electron transfer from MOF to Pt NPs than supported Pt. As a result, Pt@UiO-66-NH$_2$ exhibits much better charge-carrier utilization, and thus significantly

higher photocatalytic activity towards hydrogen production than Pt/UiO-66-NH$_2$. Furthermore, Pt@UiO-66-NH$_2$ possesses excellent stability and recyclability as a result of the great confinement for Pt NPs in the MOF.

3. Catalysis Applications

3.1. Catalytic CO Oxidation

CO oxidation has been extensively investigated in the field of heterogeneous catalysis due to the fundamental interest and its close relevance in practical applications, such as gas sensors for the detection of trace amounts of CO, automotive exhaust gas treatment, and polymer electrolyte fuel cells [37–40]. Herein, we addressed the CO oxidation reaction based on metal or metal oxide NPs/MOF composites. Table 1 summarizes the catalytic activities for CO oxidation of several MOF-supported NPs catalysts [28,41–49]. Generally, MOF-supported NPs catalysts have shown good catalytic performance for CO oxidation at relatively high temperatures.

Table 1. Catalytic activities for CO oxidations on MOF-supported nanoparticles (NPs) catalysts.

Active Species (wt %)	MOF	T_{50} [a] (°C)	T_{100} [b] (°C)	Reference
Au (5%)	ZIF-8	170	210	[41]
Au (4%)	UIO-66	155	225	[43]
Pt (5%)	NH$_2$-MIL-101(Al)	170	207	[42]
Pt (5%)	MIL-101(Cr)	118	150	[28]
Pt (5%)	*N*-UiO-67	100	120	[45]
Ag (5%)	Cu$_3$(BTC)$_2$	100	120	[48]
Pd (2.7%)	MIL-53(Al)	100	115	[44]
Pd (2.9%)	MIL-101(Cr)	92	107	[47]
Pd (5%)	Ce-MOF	77	96	[46]
Co$_3$O$_4$	ZIF-8	58	80	[49]

[a] Temperature for 50% conversion of CO into CO$_2$; [b] Temperature for 100% conversion of CO into CO$_2$.

Xu et al. [41] reported a pioneering study that described MOF-supported noble metal NPs as an efficient catalyst for CO oxidation. The catalytic activity over Au@ZIF-8 for CO oxidation increases with increasing Au loading from 0.5 to 5 wt %, accompanied by the decrease of the temperature of 50% conversion of CO from 225 °C to 170 °C. The 5 wt % Au@ZIF-8 achieves a complete conversion of CO at approximately 210 °C. Afterwards, it was reported that the total conversion of CO was achieved at around 200 °C by the Pt and Au NPs, supported on NH$_2$-MIL-101(Al) and UIO-66, respectively [42,43]. Importantly, the reaction temperature of complete conversion of CO can be further reduced to below 150 °C by incorporating Pt, Pd, and Ag NPs with apposite MOF supports [28,44–48]. Wang and co-workers proposed that both the size of the metal NPs and the nature of the support play an important role on the catalytic performance of Pt@UIO-67 for CO oxidation through a combination study of experiment and DFT calculation [45]. EL-Shall et al. [46] reported high CO oxidation activities over Pd NPs supported on Ce-MOF. The Pd@Ce-MOF catalyst with 5 wt % Pd loading shows surprisingly high catalytic activity, with a complete conversion at 96 °C. The authors proposed that the high activity was mostly attributed to the interaction of the Pd NPs and the Ce sites within Ce-MOF.

In addition to MOF-supported noble metal NPs, MOF-supported metal oxide NPs as an active catalyst for CO oxidation was reported. Wang et al. [49] firstly employed ZIF-8 as host to prepare hexagonal Co$_3$O$_4$ NPs via the thermolysis of cobalt nitrate that is accommodated in the pores of the MOF host at a low temperature of 200 °C. The Co$_3$O$_4$@ZIF-8 composite exhibited excellent catalytic activity for CO oxidation, which was related to the highly dispersed Co$_3$O$_4$ NPs in the well-retained MOF networks. Complete conversion of CO was achieved at 80 °C by the resulting composite catalyst with good cycling stability and long-term stability. Furthermore, this synthesis method can be easily extended to the preparation of other metal oxide NPs.

3.2. Catalytic CO$_2$ Conversion

Catalytic conversion of CO$_2$ into valuable chemicals, such as CO, CH$_4$, CH$_3$OH, HCOOH, cyclic carbonates, and so on, has consistently drawn significant attention [16,18,50–53]. The MOF based composites have been developed as active catalysts for the conversion of CO$_2$.

Recently, metal or metal oxide NPs incorporated in MOFs have been proved to be effective catalysts for converting CO$_2$ to valuable chemicals, including CO, CH$_4$, CH$_3$OH, and light olefins [33,53–57]. The Materials of Institute Lavoisior (MIL) and University of Oslo (UiO) families, and their surface modified MOFs were mainly used as supports due to their high thermal stability and high chemical stability in water. An efficient catalyst, which was prepared by encapsulating single Cu nanocrystal (18 nm) into UiO-66, was reported recently for CO$_2$ hydrogenation to methanol. It shows a steady eight-fold yield over the benchmark Cu/ZnO/Al$_2$O$_3$ catalyst, with a 100% selectivity to methanol [54]. Interestingly, Wang and co-workers recently extended this approach with the use of a UiO-bpy MOF, which anchored ultrafine Cu/ZnO$_x$ NPs within the pores to restrain the agglomeration of Cu NPs and phase separation between Cu and ZnO$_x$ [55]. As shown in Figure 2, the resulting Cu/ZnO$_x$@MOF catalysts exhibit remarkably higher activity (space-time yield of 2.59 g$_{MeOH}$ kg$_{Cu}^{-1}$ h^{-1}), higher selectivity (100%), and higher stability (>100 h) for methanol synthesis from CO$_2$ hydrogenation, when compared to the commercial Cu/ZnO/Al$_2$O$_3$ catalyst. Similarly, Lu et al. [33] prepared Ni NPs encapsulated in MIL-101(Cr) composites by double solvent method (DSM) and multiple impregnation method (IM) for CO$_2$ methanation. The Ni@MIL-101(DSM) catalyst with Ni loading of 20 wt % exhibited surprisingly higher activity for CO$_2$ methanation than Ni@MIL-101(IM), giving a CH$_4$ turnover frequency (TOF) value of $1.63 \times 10^{-3} \cdot s^{-1}$ at 300 °C. The author contributed the higher activity of Ni@MIL-101(DSM) to the more exposed Ni(111) facet, which was demonstrated by the result of DFT calculations that the Ni(111) plane has lower potential energy barrier (10.0 kcal/mol) for CO$_2$ dissociation into CO$_{ads}$ and O$_{ads}$ than Ni(200) facet (20.3 kcal/mol).
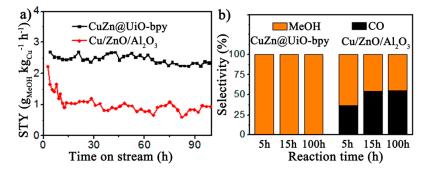

Figure 2. (**a**) The space-time yield (STY) of MeOH vs reaction time over a period of 100 h on stream; (**b**) Selectivity of product vs reaction time. Reproduced with permission from Reference [55]. Copyright 2017, American Chemical Society.

The utilization of solar energy for the conversion of CO$_2$ into valuable products is one of the best solutions to reduce carbon emission. Thus far, a range of photocatalysts, including TiO$_2$, CdS, Zn$_2$GeO$_4$, graphite-like carbon nitride (g-C$_3$N$_4$), and other compounds have been successfully combined with MOFs to photocatalytically reduce CO$_2$ [58–65]. For example, a metal-free semiconductor-composite (g-C$_3$N$_4$-ZIF-8) by growing ZIF-8 on the surface of g-C$_3$N$_4$ nanotubes for photocatalytic CO$_2$ conversion into CH$_3$OH was recently reported [63]. The ZIF-8 on the surface increases CO$_2$ capture capacity, but impairs the surface charge transfer within the photocatalytic system due to the weaker electrical conductivity. The optimized ZIF-8 modified tubular g-C$_3$N$_4$ photocatalysts show the superior catalytic performance, giving a >3-fold yield of CH$_3$OH, relative to the bulk g-C$_3$N$_4$.

The separation efficiency of the photoinduced charge carriers plays an important role in photocatalysis [18,66]. The introduction of metal atoms into MOF photocatalysts may suppress

the recombination of photoinduced electrons and holes and significantly increase their photocatalytic activity. Yaghi et al. [64] reported the construction of Ag⊂Re$_n$-MOF with enhanced photocatalytic activity for CO_2 reduction to form CO, which resulted from the cooperation of the spatially confined photoactive Re centers and the intensified near-surface electric fields at the surface of Ag nanocubes (Figure 3a). A fine balance of proximity between photoactive centers is needed for cooperatively enhanced photocatalytic activity in Re$_n$-MOFs. The optimal Re$_3$-MOF structure with the highest turnover on silver nanocubes shows a 7-fold enhancement in CO evolution rate over Re$_3$-MOF under visible light (Figure 3b). Furthermore, Ag⊂Re$_3$-MOF structure exhibits long-term stability of up to 48 h when compared to molecular H_2ReTC, and the CO produced from Ag⊂Re$_3$-MOF almost doubles from that of H_2ReTC after 48 h (Figure 3c).
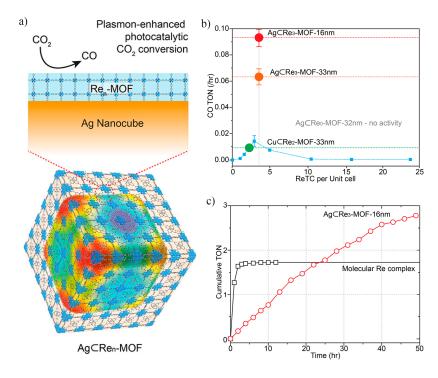

Figure 3. (**a**) Structure of Re$_n$-MOF coated on Ag nanocube for enhanced photocatalytic conversion of CO_2; (**b**) Photocatalytic CO_2-to-CO conversion activity of Re$_n$-MOFs (blue line), Ag⊂Re$_0$-MOF, Cu⊂Re$_2$-MOF, and Ag⊂Re$_3$-MOFs with MOF thickness of 16 and 33 nm; and, (**c**) Stable performance of Ag⊂Re$_3$-MOF when compared to molecular H_2ReTC. Reproduced with permission from Reference [64]. Copyright 2016, American Chemical Society.

Besides, catalytic processes that convert CO_2 into cyclic carbonates have been widely investigated due to their high atom efficiency and high value products [67,68]. A growing number of MOFs have been employed as catalysts for the formation of cyclic organic carbonate. Meanwhile, a strategy for combining MOFs with functional species, like ILs, together to form heterogeneous catalysts has been developed to enhance the catalytic activity for conversion of CO_2 into cyclic carbonates [69–71]. Shi and co-workers [72] reported two IL functionalized bifunctional catalyst, MIL-101-N(*n*-Bu)$_3$Br and MIL-101-P(*n*-Bu)$_3$Br, as prepared by the covalent post functionalization of MOFs (Figure 4a). Due to the synergy of two functional sites including Lewis acid sites in the MOF framework and nucleophilic anion in the ILs, the MIL-101-N(*n*-Bu)$_3$Br, and MIL-101-P(*n*-Bu)$_3$Br catalysts showed the highest yield to propylene carbonate (PC) (>98%) for the cycloaddition reaction of CO_2 and propylene oxide (PO), when compared to other MOFs under mild and co-catalyst free conditions (Figure 4b). Similarly, the catalytic activity of ILs supported ZIF-90 for the PO-CO_2 cycloaddition reaction is remarkably enhanced as compared to ZIF-90 [73].
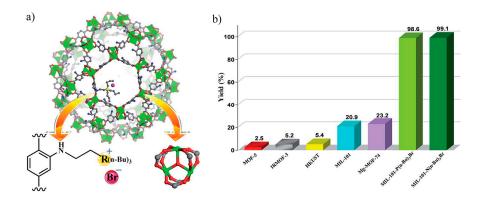
Figure 4. (**a**) The structure of the catalysts MIL-101-N(*n*-Bu)$_3$Br and MIL-101-P(*n*-Bu)$_3$Br (Cr: green; C: gray; O: red; N: blue; Br: amaranth, and R=N or P); (**b**) The yield of PC from the cycloaddition of PO and CO$_2$ catalyzed by different MOF catalysts. Reproduced with permission from Reference [72]. Copyright 2015, The Royal Society of Chemistry.

3.3. Catalytic Hydrogen Production

3.3.1. Catalytic Hydrogen Generation from Chemical Hydrides

A number of metal NPs that were immobilized in MOFs with high catalytic activities have been investigated for hydrogen generation from liquid chemical hydrides, such as aqueous formic acid (HCOOH), ammonia borane (NH$_3$BH$_3$), and hydrazine (N$_2$H$_4$). Due to the high specific surface area and tunable pore size, the loading of metal NPs inside MOFs could control the size of NPs in the confined cavities and produce monodispersed metal NPs, affording an enhanced catalytic performance.

In 2011, it was reported firstly that bimetallic Au-Pd NPs immobilized into MIL-101 and ethylenediamine (ED)-grafted MIL-101 (ED-MIL-101) were efficient catalysts for the hydrogen generation from formic acid at a mild temperature [74]. The obtained Au-Pd/ED-MIL-101 catalyst (Au-Pd loading: 20.4 wt %; Au:Pd = 2.46) exhibits superior catalytic performance when compared to those of other counterparts, giving a TOF of 106 h^{-1} at 90 °C. The enhanced activity is contributed to the smaller particle sizes of the Au-Pd alloy by the introduction of the electron-rich ED into MIL-101 and the strong synergistic effects between Au and Pd. This study reveals a new approach to immobilize metal NPs for hydrogen generation from formic acid. Since then, metal NPs, including monometallic NPs, bimetallic NPs, and even trimetallic NPs that were supported on various MOFs for hydrogen generation have been widely investigated [28–32,74–91]. Table 2 summarizes the catalytic activities of different catalysts for hydrogen production from HCOOH, NH$_3$BH$_3$, and hydrazine. Among these MOF-supported metal NPs catalyst, the Au$_{0.28}$Pd$_{0.47}$Co$_{0.25}$/MIL-101-NH$_2$ catalyst exhibits 100% selectivity to H$_2$ and the drastically high activity for the dehydrogenation of formic acid at room temperature with a TOF value of 347 h^{-1} [86]. Interestingly, Yamashita and co-workers [91] recently reported the use of the synergistic catalysis of plasmonic Au@Pd NPs, and Ti-doped amine functionalized MOFs for enhancing hydrogen production from formic acid at room temperature. As shown in Figure 5, the activity of all supported Au@Pd catalysts is greatly enhanced under visible light irradiation, and the Au@Pd/UiO-66(Zr$_{85}$Ti$_{15}$) shows better catalytic performance under visible light irradiation when compared to those under dark conditions, giving a high TOF of 200 h^{-1}. The similar cooperative promoting effect from both NPs and photoactive MOF was examined on a noble-metal-free catalyst Ni@MIL-101 for hydrogen generation from ammonia borane under assistance of visible light irradiation [88].
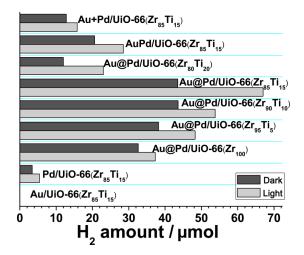
Figure 5. Amount of H_2 produced through formic acid dehydrogenation in the dark (black bars) or under visible light irradiation (gray bars, $\lambda > 420$ nm, 320 mW·cm^{-2}) over different catalysts. Reproduced with permission from Reference [91]. Copyright 2017, American Chemical Society.

Table 2. Catalytic activities of different catalysts for hydrogen generation from chemical hydrides.

Catalyst	Chemical Hydrides	T (°C)	TOF (h^{-1})	Refernece
AuPd@ED-MIL-101	HCOOH	90	106	[74]
Ag$_{20}$Pd$_{80}$@MIL-101	HCOOH	80	848	[79]
Ag$_{18}$Pd$_{82}$@ZIF-8	HCOOH	80	580	[82]
Au$_{28}$Pd$_{47}$Co$_{25}$/MIL-101–NH$_2$	HCOOH	25	347	[86]
Ag$_{25}$Pd$_{75}$@NH$_2$-UIO-66	HCOOH	25	103	[87]
Au@Pd/NH$_2$-UiO-66(Zr$_{85}$Ti$_{15}$)	HCOOH	30	200	[91]
Ni@ZIF-8	NH$_3$BH$_3$	25	504	[75]
Ru@MIL-101	NH$_3$BH$_3$	25	10680	[77]
Ni@MIL-101	NH$_3$BH$_3$	25	3238	[88]
Pd@Co@MIL-101	NH$_3$BH$_3$	30	3060	[81]
Au$_7$Ni$_{93}$ @MIL-101	NH$_3$BH$_3$	25	3972	[29]
Ru$_{30}$Ni$_{70}$@MIL-101	NH$_3$BH$_3$	25	16363	[30]
Au$_6$Co$_{94}$@MIL-101	NH$_3$BH$_3$	25	1410	[31]
Cu$_{30}$Co$_{70}$@MIL-101	NH$_3$BH$_3$	25	1176	[32]
CuCo@MIL-101	NH$_3$BH$_3$	25	3102	[90]
FeCo@MIL-101	NH$_3$BH$_3$	25	3048	[90]
NiCo@MIL-101	NH$_3$BH$_3$	25	2658	[90]
Ni$_{80}$Pt$_{20}$@ZIF-8	Hydrazine	50	90	[76]
Ni$_{66}$Rh$_{34}$@ZIF-8	Hydrazine	50	140	[80]
Ni$_{88}$Pt$_{12}$@MIL-101	Hydrazine	50	375	[78]
Ni$_{42}$Rh$_{58}$@MIL-101	Hydrazine	50	344	[84]
Ni$_{85}$Ir$_{15}$@MIL-101	Hydrazine	50	464	[85]

In order to reduce the deposition of the metal NPs on the outer surface of MOF support, Xu et al. [28] successfully developed a double solvent approach combined with hydrogen reduction to immobilize the ultrafine Pt NPs inside the pores of MIL-101. The resulting Pt@MIL-101 composite with 2 wt % Pt loading is highly active for H_2 generation from aqueous ammonia borane at room temperature. By using a similar approach, AuNi [29], RuNi [30], AuCo [31], and CuCo [32] alloy NPs are also successfully encapsulated in the pores of MIL-101. The resulting MIL-101 supported bimetallic NPs catalysts present remarkably high catalytic activity for hydrolytic dehydrogenation of ammonia borane, giving the highest TOF of 66.2 min^{-1}, 272.7 min^{-1}, 23.5 min^{-1}, and 19.2 min^{-1}, respectively.

The hydrogen generation from the dehydrogenation of hydrous hydrazine has also been investigated using MOF-supported bimetallic NPs catalysts with high selectivity [76,78,80,84,85]. Highly dispersed bimetallic Ni-Pt NPs are successfully immobilized onto ZIF-8 via a facile liquid

impregnation method, followed by co-reduction [76]. The activity of the composite catalysts strongly depended on the Ni-Pt composition, and the catalyst $Ni_{80}Pt_{20}$/ZIF-8 exhibits the highest activity at 50 °C with a 100% hydrogen selectivity and a TOF value of 90 h^{-1}. Following a similar approach, Luo and his co-workers [78,80,84,85] successfully encapsulated the bimetallic Ni-Pt, Ni-Rh, and Ni–Ir NPs with different compositions into the cavities of ZIF-8 and MIL-101. The optimal catalysts, $Ni_{88}Pt_{12}$@MIL-101 [78], $Ni_{66}Rh_{34}$@ZIF-8 [80], $Ni_{42}Rh_{58}$@MIL-101 [84], and $Ni_{85}Ir_{15}$@MIL-101 [85], enable the rapid and complete decomposition of hydrazine in an aqueous alkaline solution, with a 100% H$_2$ selectivity at 50 °C, giving the highest TOF value of 375.1 h^{-1}, 140 h^{-1}, 344 h^{-1}, and 464 h^{-1}, respectively.

3.3.2. Catalytic Hydrogen Production from Water

The photocatalytic water splitting is an ideal method for producing hydrogen. Developing new hybrid photocatalysts combined with MOFs is considered to improve the charge transfer/separation efficiency. Some researchers incorporate Pt NPs into MOFs to enhance hydrogen evolution reaction (HER) activity [36,92,93]. For example, approximately 3 nm Pt NPs are incorporated into or supported on UiO-66-NH$_2$, to afford Pt@UiO-66-NH$_2$ and Pt/UiO-66-NH$_2$, respectively (Figure 6a) [36]. A high H$_2$ evolution rate of 257.38 $\mu mol \cdot g^{-1} \cdot h^{-1}$, which is approximately 150 and 5 times higher than that of the parent MOF and the Pt/UiO-66-NH$_2$, respectively, was achieved using a Pt@UiO-66-NH$_2$ photocatalyst with the optimum Pt loading amount (2.87 wt %) (Figure 6b). In addition, as shown in Figure 6c, the Pt@UiO-66-NH$_2$ shows better catalytic recyclability than that of Pt/UiO-66-NH$_2$ because Pt@UiO-66-NH$_2$ effectively restrains aggregation or leaching of Pt NPs during the reaction.
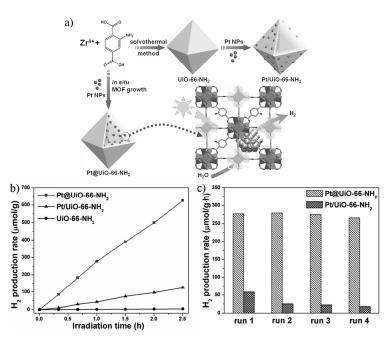

Figure 6. (**a**) Schematic illustration for the synthesis of Pt@UiO-66-NH$_2$ and Pt/UiO-66-NH$_2$; (**b**) The photocatalytic hydrogen-production rates of UiO-66-NH$_2$, Pt@UiO-66-NH$_2$, and Pt/UiO-66-NH$_2$; and, (**c**) Recycling performance comparison between Pt@UiO-66-NH$_2$ and Pt/UiO-66-NH$_2$. Reproduced with permission from Reference [36]. Copyright 2016, John Wiley & Sons, Inc.

Recently, some functional components, including nickel particles [94], metal sulfides (e.g., MoxSy, NixSy, CdS) [95–98], reduced graphene oxide (rGO) [99], g-C$_3$N$_4$ [100], and POMs [101] have been employed to replace precious Pt and improve the photocatalytic activity for HER. Excellent photocatalytic activity was achieved as well. Interestingly, MoS$_2$ increases the photoactivity for

the HER and was superior to Pt as a co-catalyst [96]. 1 wt % MoS_2/UiO-66-CdS obtained a high H_2 evolution rate of 25,770 $\mu mol \cdot g^{-1} \cdot h^{-1}$, approximately 2-fold higher than that of 1 wt % Pt/UiO-66-CdS. Lin et al. [101] reported the successful encapsulation of tetra-nickel-containing Ni_4P_2 POMs into the pores of highly stable MOFs. The integration of the photosensitizing MOF framework and the POM catalyst allows for facile multi-electron transfer to enable an efficient HER, with turnover numbers as high as 1476.

3.4. Organic Reactions

3.4.1. Oxidation of Alcohols and Hydrocarbons

MOF composites have been employed as efficient catalysts for the selective oxidation of alcohols, which are commonly considered as the central reactions in organic chemistry. Li et al. [102–104] investigated the catalytic performance of a series of MOF composites that were fabricated with different metal NPs (Au, Pd, and Pt) in liquid-phase aerobic oxidation of alcohols. The resulting Au/MIL-101, Pd/UIO-67, and Pt/DUT-5 composite catalysts exhibit excellent catalytic activities in a variety of alcohols oxidation reactions under base-free conditions, with exceeding 99% conversions and up to 100% selectivity to cinnamyl aldehyde. The authors attributed the superior catalytic activity to the beneficial synergetic effects of the electron donation and nano-confinement that is offered by the MOF framework.

Other composite systems, including Au NPs, metal nanoclusters, POMs, CdS, and rGO, also exhibit high catalytic activities for selective oxidation of various alcohol substrates to aldehydes [105–111]. For example, Zhu et al. [106] recently reported the atomically precise nanoclusters@MIL-101 composites, prepared by using MOFs as the size-confining templates for the first time. Highly dispersed $Au_{13}Ag_{12}$@MOF composites exhibited favorable catalytic activity in the oxidation of benzyl alcohol toward benzaldehyde, exceeding 75% conversion and 100% selectivity.

Besides, the aerobic oxidation of hydrocarbons catalyzed by MOF based nanohybrid catalysts has also been explored. Various active species, including Au, AuPd, PtPd alloy NPs, POMs, and grapheme oxide (GO), combined with several MOFs were proved to be active and selective in the oxidation hydrocarbons with molecular oxygen [108,112–115]. For example, the AuPd/MIL-101 catalyst exhibited a superior activity and selectivity in the oxidation of cyclohexane to cyclohexanone and cyclohexanol (KA-oil) when compared with those of their pure metal counterparts and an Au+Pd physical mixture, which may be correlated to the synergistic alloying effect of bimetallic AuPd NPs [113]. Cyclohexane conversion exceeding 40% is achieved (TOF = 19,000 h^{-1}) with >80% selectivity to KA-oil under mild solvent-free conditions. Recently, $H_{3+x}PMo_{12-x}V_xO_{40}$@MIL-100 (Fe) ($x$ = 0, 1, 2) hybrids were prepared by the encapsulation of POMs within a metal–organic framework using a hydrothermal method [116]. The hybrids show greatly improved catalytic performance for the allylic oxidation of cyclohexene using H_2O_2 as green oxidant. In particular, the hybrid $H_4PMo_{11}VO_{40}$@MIL-100 (Fe) leads to 85% cyclohexene conversion, 91% selectivity for 2-cyclohexene-1-one under optimized conditions, as well as excellent stability and reusability.

3.4.2. Hydrogenation Reaction

Hydrogenation is a key reaction that is extensively employed in industry. The Pd, Pt, Ru, and Ni NPs, and their bimetallic NPs immobilized by MOFs have been proven to be active catalysts in the hydrogenation of a wide range of substrates including alkenes [117–120], alkynes [121,122], aromatics [123], nitro-aromatics [124,125], ketones [126], aldehydes [127,128], and other compounds [129,130].

When considering the molecular sieving capability of the pore apertures of MOFs, the encapsulated metal NPs in the internal frameworks of MOFs have been demonstrated to exhibit interesting size selectivity for the hydrogenation of different alkenes [25,131,132]. For example, Jiang et al. [24] reported the beneficial combination of the photothermal effects of metal

nanocrystals with the favorable properties of MOFs for efficient and selective catalysis. As shown in Figure 7a, the Pd nanocubes (NCs)@ZIF-8 composite shows significantly different catalytic activity for olefins with different molecular sizes. For *n*-hexene, approximately 100% conversion can be achieved, while large molecules, such as cyclooctene (5.5 Å), cannot access the ZIF-8 shell with a pore aperture of (3.4 Å), resulting in negligible conversion. More interestingly, the catalytic performance of the Pd NCs@ZIF-8 composite in the hydrogenation of *n*-hexene is significantly improved by light irradiation (Figure 7b).
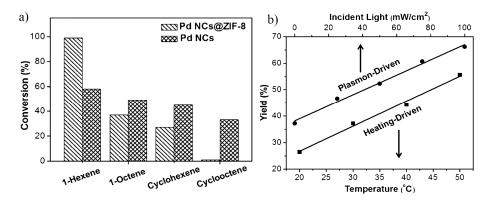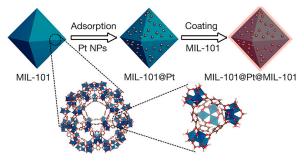

Figure 7. (**a**) Conversions of the hydrogenation of various alkenes over Pd NCs@ZIF-8 and Pd NCs under 100 mWcm^{-2} full-spectrum irradiation at room temperature; (**b**) The yields of the hydrogenation of 1-hexene with 1atm H$_2$ over Pd NCs@ZIF-8 under full-spectrum irradiation with different light intensities at room temperature or upon heating at different temperatures. Reproduced with permission from Reference [24]. Copyright 2016, John Wiley & Sons, Inc.

Recently, Zhao and co-workers [128] successfully fabricated a sandwich nanostructured catalyst with a layer of Pt NPs encapsulated between a core and a shell made of MIL-101 (Figure 8). The MIL-101(Cr)@Pt@MIL-101(Fe) catalyst, with a shell of thickness 2.9 nm, exhibits excellent selectivity (95.6%) and almost full conversion (99.8%) for the selective hydrogenation of cinnamaldehyde to cinnamyl alcohol. Furthermore, the shell thickness in sandwich nanostructures can be used to tune the activity and selectivity of sandwich-type catalysts. The design of a sandwich nanostructured catalyst provides a potential strategy for designing selective catalysts for many important, but highly challenging, reactions.

Figure 8. Synthetic route to generating sandwich MIL-101@Pt@MIL-101. Reproduced with permission from Reference [128]. Copyright 2016, Nature Publishing Group.

3.4.3. Catalytic C-C Coupling

C–C coupling reactions, including Suzuki-Miyaura, Ullmann, Heck, Sonogashira, and Stille reactions are among the most versatile and important reactions in organic synthesis [20]. Pd is the

most common catalyst in promoting these coupling reactions, and hence MOF supported Pd NPs have been developed as C–C coupling catalysts [133–136]. Trzeciak and his co-workers [137] synthesized the supported Pd NPs on a nanoscale Ni-MOF by using a facile impregnation process with solvent in situ reduction method, which was confirmed as a highly active heterogeneous catalyst for the Suzuki-Miyaura coupling reaction between aryl halides and phenylboronic acid. This composite catalyst gives high yields of different coupling products with good recycle stability, indicating the excellent performance of the catalyst.

3.5. Catalytic Remediation of Pollutants

Wastewater that is produced in many industrial processes often contains toxic organic compounds and heavy metals, including organic dyes, phenols, hydrocarbons, pharmaceuticals, hexavalent chromium (Cr(VI)), and so on. It is necessary to reduce the concentration of pollutants before discharging the wastewater into the aquatic environment. Otherwise, various environmental and health issues could be induced. Among the physical, chemical, and biological technologies that are applied for the removal of pollutants, heterogeneous catalysis, including photocatalysis, has been demonstrated to be an efficient, economical, and green technique to degrade pollutants into easily biodegradable or less toxic compounds. Recently, MOF based composites with noble metal NPs, metal oxide/sulfides, GO, and other compounds have been proved to be a new class of catalysts, which are usable in the catalytic degradation of organic pollutants and Cr(VI) [138–159].

3.5.1. Catalytic Degradation of Organic Pollutants

Advanced oxidation processes (AOPs) are increasingly adopted for the degradation of organic pollutants, owing to the in situ generation of highly reactive and nonselective radicals, such as $^\bullet$OH, $^\bullet O_2{}^-$, $^\bullet$OOH, and $^\bullet SO_4{}^-$ [160]. In AOPs, heterogeneous photocatalysis has been developed to be a green and efficient approach to degrade various organic pollutants. Since the amenability to design MOFs by controlling the constituent metal ions and organic linkers, MOFs-based photocatalysts with various morphology and structure have a great potential in the degradation of organic pollutants and environmental remediation.

Qiu et al. [154] firstly rationally fabricated a new type of core–shell Fe_3O_4@MIL-100(Fe) composite with a magnetic core and a designable MOF shell. This magnetic recyclable composite exhibits photocatalytic activity for methylene blue (MB) degradation under both UV-vis and visible light irradiation with good recycling stability. Based on a similar process, a yolk-shell Co_3O_4@MOF was successfully prepared via the fabrication of a uniform Fe-doped MOF-5 shell around Co_3O_4 NPs [150]. The degradation rate of 4-chlorophenol in the presence of peroxymonosulfate over 99% within 60 min was achieved by the Co_3O_4@MOF composite with satisfactory reusability.

Recently, Yuan et al. [142] reported a novel core–shell In_2S_3@MIL-125(Ti) photocatalytic adsorbent, which was prepared by a facile solvothermal method. The integrated composite exhibits excellent adsorption affinity, as well as superior photocatalytic activity, for the removal of tetracycline (TC). The photo-degradation efficiency for TC within a 60-min visible light irradiation is 63.3%, which is much higher than that of bare In_2S_3 or MIL-125(Ti), indicating the beneficial synergistic effect between MIL-125(Ti) and In_2S_3. The core–shell composites also reveal good performance for the removal of TC from various real wastewaters. Similarly, the CdS/MIL-53(Fe) and CdTe QDs/Eu-MOF composites show high photocatalytic activity in the degradation of Rhodamine B (RhB) and Rhodamine 6G in water at room temperature under light irradiation [143,146].

Alternatively, the bismuth oxyhalides (BiO*X*, *X* = Cl, Br, I) and MOFs composites are also effective in improving photocatalytic performance. BiOBr/UIO-66, BiOBr/NH$_2$-MIL125(Ti), BiOBr/CAU-17, and BiOI/MIL-88B(Fe) nanocomposites have been reported as highly efficient photocatalysts for the degradation of organic pollutants [147–149,158].

Unlike metal semiconductor photocatalysts, g-C_3N_4, a metal-free semiconductor, has been successfully employed as a semiconductor photocatalyst for pollutant degradation [141,144].

Yuan et al. [141] successfully combined g-C_3N_4 with MIL-125(Ti) by a facile solvothermal method. The resulting g-C_3N_4/MIL-125(Ti) composite catalyst exhibits an excellent catalytic performance with good reusability and stability. The optimal photocatalytic performance is obtained at the g-C_3N_4 content of 7 wt % for MIL-125(Ti), on which the rate of RhB photodegradation is 0.0624 min^{-1}, which is about 2.1 and 24 times higher than that of pure g-C_3N_4 and MIL-125(Ti), respectively.

3.5.2. Catalytic Cr(VI) Reduction

Catalytic reductive transformation of Cr(VI) to Cr(III) is a promising method to perform effective remediation of Cr(VI), because Cr(III) is much less toxic and can be easily precipitated and removed due to its lower solubility in water in contrast to highly water-soluble and toxic Cr(VI).

Xu, Yu and Trivedi's groups reported active MOF-supported noble metal (Pt, Pd) NPs catalysts for the reduction of Cr(VI) to Cr(III) using formic acid [145,152,157]. The resulting composites exhibit favorable catalytic performance, as demonstrated by the short time of complete reduction of Cr(VI) into Cr(III). Importantly, Yu et al. [152] proposed a reasonable mechanism for the catalytic reduction of Cr(VI) into Cr(III), as evidenced by a series of experiments. Formic acid is first adsorbed on the surface of metal NPs, and is then is dehydrogenated to produce H_2 and CO_2, according to Equation (1). The generated hydrogen, with high reduction capacity, then reduces Cr(VI) into Cr(III), as shown in Equation (2):

$$HCOOH \rightarrow H_2 + CO_2 \tag{1}$$

$$Cr_2O_7{}^{2-} + 8H^+ + 3H_2 \rightarrow 2Cr^{3+} + 7H_2O \tag{2}$$

Wu et al. [155] firstly reported the simultaneous degradation of different categories of pollutants, such as Cr(VI) and organic dyes, by using MOF-supported Pd NPs as a dual functional photocatalyst. As shown in Figure 9a, Pd@UiO-66-NH_2 is highly active to almost completely reduce Cr(VI) into Cr(III) within 90 min under visible light irradiation ($\lambda \geq$ 420 nm) at a pH range of 1–5, which is ascribed to the intimate interfacial contact between Pd and UiO-66-NH_2, leading to the efficient charge separation. More interestingly, the reduction of Cr(VI) is visibly enhanced when the organic dye (MB or methyl orange (MO)) is added into the reaction system. In the binary systems of Cr(VI)/MO and Cr(VI)/MB, the reduction ratios of Cr(VI) are 79% and ~100%, respectively, which are obviously higher than that in the single system (70%) (Figure 9b). Meanwhile, the presence of Cr(VI) also promotes the photocatalytic degradation of MB and MO, demonstrating the beneficial synergic effect between the photocatalytic reduction and oxidation process. Wu et al. [138] also reported that the MIL-53(Fe)-rGO composite exhibits high photocatalytic activity in simultaneous oxidation of organic dyes and the reduction of Cr(VI).
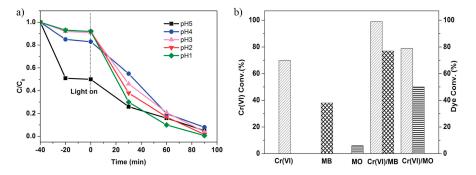

Figure 9. (**a**) Photocatalytic reduction of aqueous hexavalent chromium (Cr(VI)) with different amounts of H_2SO_4 solution (0.2 M); and (**b**) Simultaneous photocatalytic reduction of Cr(VI) and degradation of dyes (10 ppm) over Pd@UiO-66-NH_2 under visible light irradiation ($\lambda \geq$ 420 nm). Reproduced with permission from Reference [155]. Copyright 2013, The Royal Society of Chemistry.

Moreover, the rGO-UiO-66-NH$_2$ and rGO-MIL-53(Fe) nanocomposites were successfully assembled by electrostatic attractive force for surface attachment [138,159]. The optimal photocatalytic performance is obtained at the rGO content of 2% and 0.5% for UiO-66-NH$_2$ and MIL-53(Fe), for which the reduction ratio of Cr(VI) is even up to 100% under visible light illumination within 100 min and 80 min, respectively.

Recently, Wang et al. [139] employed ZnO colloidal spheres as template and zinc source to successfully fabricate core-shell ZnO@ZIF-8 composite. The resulting composite exhibits an enhanced selective photocatalytic reduction of Cr(VI) between Cr(VI) and MB, which is attributed to selective adsorption and permeation effect of the ZIF-8 shell.

4. Conclusions and Outlook

MOFs have been considered as ideal catalysts with clearly defined and designable crystal structures, high surface areas, tunable and uniform pore structures, and special confined nanopore microenvironments [27]. Some intrinsic weaknesses (like the lack in the catalytically active sites and limited thermal and chemical stability), however, hinder them from implementing the full potential for catalyst uses. With the improvement of the MOF syntheses, MOFs with enhanced thermal and chemical stability have been more and more available [9,14,27,35]. To enhance the catalytic properties of MOFs, MOF based metal and metal oxide NP composites have been prepared and successfully applied for many reactions. The "ship in bottle" strategy, "bottle around ship" strategy, and one-step synthesis strategy have been exploited for the syntheses of such composites. Among these strategies, the "ship in bottle" approach has some limitations in the precise control of the size, morphology, and composition of incorporated NPs. On the contrary, the size, morphology, and composition of NPs can be better controlled with the "bottle around ship" approach. The one-step approach is straightforward, but it usually needs the functional groups in organic linkers or solvents to trap the NPs precursors and stabilize the NPs that are formed.

The present studies have demonstrated that the MOF based NP composite catalysts exhibit excellent catalytic performances for CO oxidation, CO$_2$ conversion, hydrogen production, organic reaction, and pollutant degradation. The high catalytic performances are contributed to the beneficial synergistic effects of MOFs and active sites of NPs. Significantly increasing applications of MOF based NP composite catalysts can be expected.

However, MOF composites, as heterogeneous catalysts, are still under its early developing stage. In the view of structural features, MOF composites consist of active species, metal ions and organic ligands, which are the potential factors influencing the catalytic performance. The relationship between the catalytic behavior and the structural features still needs to be investigated further. Further improvement in the thermal and chemical stability of MOFs is required. The present syntheses of MOFs are not cheap. Some syntheses are complex and time consuming, with difficulty in the scaling up. Innovation in the syntheses of MOFs is one of the future developments. Besides the improvement in the syntheses of MOFs for catalyst uses, the following studies are expected to further lead the progresses in the MOF composite catalysts:

(1) A principal advantage of MOFs is their designable structure with clear chemistry. When metal or metal oxide NPs are introduced, not clear chemistry may be caused because of not only various complex issues of NPs (like defects), but the interaction between MOFs and NPs. This is the most significant challenge for the future development with opportunities. In order to develop a size, structure, and location controllable preparation of NP/MOF composites, the interaction between metal or metal oxide and the MOF support needs to be further investigated. The functionalization and modification of MOFs needs to be also further investigated. The involvement of organic links in the catalytic reaction and the formation of intrinsic structure of MOFs with NPs generate many fundamental thermodynamic and kinetic issues for catalyst investigations. The reported studies are mostly limited within the experimental exploitation of MOFs for various reactions. Regarding the difficulty in the catalyst characterization, more theoretical studies are needed [45,161,162].

(2)   For the composites by the pre-synthesized NPs, the polymer capping agent, like PVP, has some negative effects on the catalytic properties. Alternatives to such agents should be investigated. In this regard, biomolecules, like peptide, can be a nice candidate [163–165]. Especially, the peptide metal composite can serve as an excellent nitrogen dopant, which will be good for the improvement of the electronic properties of the catalysts, especially, for photocatalyst and electro-photocatalyst.

(3)   Since MOFs are now mostly thermal sensitive materials, innovation in the post treatment or modification of the NP/MOF composites at low temperatures is extremely important. We attempted to use the room temperature electron reduction [166,167] for the preparation of noble metal/MOF composite catalyst. The present result shows the NPs cannot disperse well into the pores of MOFs. Further improvement is required. Other new approaches are also needed.

(4)   An important future direction is the preparation of NP/MOF composites, together with gels, graphene, porous polymers, ionic liquids, and others, especially for the blooming photocatalytic and photo-electro-catalytic applications [168,169].

(5)   The development of MOF based solid acid and solid base will create more opportunities for NP/MOF composite catalysts [170].

(6)   MOF itself has been demonstrated to be an excellent single site catalyst, with which metal nodes in MOFs mimic homogeneous catalysts not only functionally but also mechanistically [171,172]. It provides a blueprint for the development of advanced heterogeneous catalysts with similar degrees of tunability to their homogeneous counterparts. It could open new ways for the investigations of NP/MOF catalysts or MOF supported NP catalysts, which possess characteristics and advantages of both heterogeneous and homogeneous catalysts.

Author Contributions: W.X. contributed to writing and designing the article. Y.Z., H.L. and C.-j.L. contributed critical revisions to the article and intellectual discussions.

Conflicts of Interest: The authors declare no conflict of interest.

References

1.   Liu, X.W.; Sun, T.J.; Hu, J.L.; Wang, S.D. Composites of metal–organic frameworks and carbon-based materials: Preparations, functionalities and applications. *J. Mater. Chem. A* **2016**, *4*, 3584–3616. [CrossRef]

2.   Ricco, R.; Malfatti, L.; Takahashi, M.; Hill, A.J.; Falcaro, P. Applications of magnetic metal-organic framework composites. *J. Mater. Chem. A* **2013**, *1*, 13033–13045. [CrossRef]

3.   Li, S.Z.; Huo, F.W. Metal–organic framework composites: From fundamentals to applications. *Nanoscale* **2015**, *7*, 7482–7501. [CrossRef] [PubMed]

4.   Kitao, T.; Zhang, Y.Y.; Kitagawa, S.; Wang, B.; Uemura, T. Hybridization of MOFs and polymers. *Chem. Soc. Rev.* **2017**, *46*, 3108–3133. [CrossRef] [PubMed]

5.   Wu, C.D.; Zhao, M. Incorporation of Molecular Catalysts in Metal-Organic Frameworks for Highly Efficient Heterogeneous Catalysis. *Adv. Mater.* **2017**, *29*, 1605446. [CrossRef] [PubMed]

6.   Furukawa, H.; Cordova, K.E.; O'Keeffe, M.; Yaghi, O.M. The Chemistry Applications of Metal-Organic Frameworks. *Science* **2013**, *341*, 1230444. [CrossRef] [PubMed]

7.   Yu, J.; Mu, C.; Yan, B.; Qin, X.; Shen, C.; Xue, H.; Pang, H. Nanoparticle/MOF composites: Preparations and applications. *Mater. Horiz.* **2017**, *4*, 557–569. [CrossRef]

8.   Dhakshinamoorthy, A.; Asiri, A.M.; Garcia, H. Metal Organic Frameworks as Versatile Hosts of Au Nanoparticles in Heterogeneous Catalysis. *ACS Catal.* **2017**, *7*, 2896–2919. [CrossRef]

9.   Yang, Q.; Xu, Q.; Jiang, H.L. Metal-organic frameworks meet metal nanoparticles: Synergistic effect for enhanced catalysis. *Chem. Soc. Rev.* **2017**, *46*, 4774–4808. [CrossRef] [PubMed]

10. Du, D.Y.; Qin, J.S.; Li, S.L.; Su, Z.M.; Lan, Y.Q. Recent advances in porous polyoxometalate-based metal-organic framework materials. *Chem. Soc. Rev.* **2014**, *43*, 4615–4632. [CrossRef] [PubMed]

11. Falcaro, P.; Ricco, R.; Yazdi, A.; Imaz, I.; Furukawa, S.; Maspoch, D.; Ameloot, R.; Evans, J.D.; Doonan, C.J. Application of metal and metal oxide nanoparticles@MOFs. *Coord. Chem. Rev.* **2016**, *307*, 237–254. [CrossRef]

12. Ren, Y.; Wang, M.; Chen, X.; Yue, B.; He, H. Heterogeneous Catalysis of Polyoxometalate Based Organic-Inorganic Hybrids. *Materials* **2015**, *8*, 1545–1567. [CrossRef] [PubMed]

13. Fujie, K.; Otsubo, K.; Ikeda, R.; Yamada, T.; Kitagawa, H. Low temperature ionic conductor: Ionic liquid incorporated within a metal–organic framework. *Chem. Sci.* **2015**, *6*, 4306. [CrossRef]

14. Chen, Z.; Chen, J.; Li, Y. Metal–organic-framework-based catalysts for hydrogenation reactions. *Chin. J. Catal.* **2017**, *38*, 1108–1126. [CrossRef]

15. Lian, X.; Fang, Y.; Joseph, E.; Wang, Q.; Li, J.; Banerjee, S.; Lollar, C.; Wang, X.; Zhou, H.C. Enzyme-MOF (metal-organic framework) composites. *Chem. Soc. Rev.* **2017**, *46*, 3386–3401. [CrossRef] [PubMed]

16. Ye, J.; Liu, C.-J. Cu$_3$(BTC)$_2$: CO oxidation over MOF based catalysts. *Chem. Commun.* **2011**, *47*, 2167–2169. [CrossRef] [PubMed]

17. Wang, C.C.; Du, X.D.; Li, J.; Guo, X.X.; Wang, P.; Zhang, J. Photocatalytic Cr(VI) reduction in metal-organic frameworks: A mini-review. *Appl. Catal. B Environ.* **2016**, *193*, 198–216. [CrossRef]

18. Wang, C.C.; Zhang, Y.Q.; Li, J.; Wang, P. Photocatalytic CO$_2$ reduction in metal–organic frameworks: A mini review. *J. Mol. Struct.* **2015**, *1083*, 127–136. [CrossRef]

19. Zhang, Y.M.; Dai, T.L.; Zhang, F.; Zhang, J.; Chu, G.; Quan, C.S. Fe$_3$O$_4$@UiO-66-NH$_2$ core-shell nanohybrid as stable heterogeneous catalyst for Knoevenagel condensation. *Chin. J. Catal.* **2016**, *37*, 2106–2113. [CrossRef]

20. Dhakshinamoorthy, A.; Asiri, A.M.; Garcia, H. Metal-organic frameworks catalyzed C-C and C-heteroatom coupling reactions. *Chem. Soc. Rev.* **2015**, *44*, 1922–1947. [CrossRef] [PubMed]

21. Verma, S.; Baig, R.B.; Nadagouda, M.N.; Varma, R.S. Fixation of carbon dioxide into dimethyl carbonate over titanium-based zeolitic thiophene-benzimidazolate framework. *Sci. Rep.* **2017**, *7*, 655. [CrossRef] [PubMed]

22. Verma, S.; Baig, R.B.; Nadagouda, M.N.; Varma, R.S. Titanium-based zeolitic imidazolate framework for chemical fixation of carbon dioxide. *Green Chem.* **2016**, *18*, 4855–4858. [CrossRef]

23. Liu, Y.X.; Geng, Y.Y.; Yan, M.Y.; Huang, J. Stable ABTS Immobilized in the MIL-100(Fe) Metal-Organic Framework as an Efficient Mediator for Laccase-Catalyzed Decolorization. *Molecules* **2017**, *22*, 920. [CrossRef] [PubMed]

24. Yang, Q.; Xu, Q.; Yu, S.H.; Jiang, H.L. Pd Nanocubes@ ZIF-8: Integration of Plasmon-Driven Photothermal Conversion with a Metal-Organic Framework for Efficient and Selective Catalysis. *Angew. Chem. Int. Ed.* **2016**, *55*, 3685–3689. [CrossRef] [PubMed]

25. Li, Z.; Yu, R.; Huang, J.; Shi, Y.; Zhang, D.; Zhong, X.; Wang, D.; Wu, Y.; Li, Y. Platinum-nickel frame within metal-organic framework fabricated in situ for hydrogen enrichment and molecular sieving. *Nat. Commun.* **2015**, *6*, 8248. [CrossRef] [PubMed]

26. Zhu, Q.L.; Xu, Q. Metal-organic framework composites. *Chem. Soc. Rev.* **2014**, *43*, 5468–5512. [CrossRef] [PubMed]

27. Zhang, Y.P.; Zhou, Y.; Zhao, Y.; Liu, C.J. Recent progresses in the size and structure control of MOF supported noble metal catalysts. *Catal. Today* **2016**, *263*, 61–68. [CrossRef]

28. Aijaz, A.; Karkamkar, A.; Choi, Y.J.; Tsumori, N.; Ronnebro, E.; Autrey, T.; Shioyama, H.; Xu, Q. Immobilizing highly catalytically active Pt nanoparticles inside the pores of metal-organic framework: A double solvents approach. *J. Am. Chem. Soc.* **2012**, *134*, 13926–13929. [CrossRef] [PubMed]

29. Zhu, Q.L.; Li, J.; Xu, Q. Immobilizing metal nanoparticles to metal-organic frameworks with size and location control for optimizing catalytic performance. *J. Am. Chem. Soc.* **2013**, *135*, 10210–10213. [CrossRef] [PubMed]

30. Roy, S.; Pachfule, P.; Xu, Q. High Catalytic Performance of MIL-101-Immobilized NiRu Alloy Nanoparticles towards the Hydrolytic Dehydrogenation of Ammonia Borane. *Eur. J. Inorg. Chem.* **2016**, *2016*, 4353–4357. [CrossRef]

31. Li, J.; Zhu, Q.L.; Xu, Q. Highly active AuCo alloy nanoparticles encapsulated in the pores of metal-organic frameworks for hydrolytic dehydrogenation of ammonia borane. *Chem. Commun.* **2014**, *50*, 5899–5901. [CrossRef] [PubMed]

32. Li, J.; Zhu, Q.L.; Xu, Q. Non-noble bimetallic CuCo nanoparticles encapsulated in the pores of metal-organic frameworks: Synergetic catalysis in the hydrolysis of ammonia borane for hydrogen generation. *Catal. Sci. Technol.* **2015**, *5*, 525–530. [CrossRef]

33. Zhen, W.; Gao, F.; Tian, B.; Ding, P.; Deng, Y.; Li, Z.; Gao, H.; Lu, G. Enhancing activity for carbon dioxide methanation by encapsulating (1 1 1) facet Ni particle in metal–organic frameworks at low temperature. *J. Catal.* **2017**, *348*, 200–211. [CrossRef]

34. Aguilera-Sigalat, J.; Bradshaw, D. Synthesis and applications of metal-organic framework-quantum dot (QD@MOF) composites. *Coord. Chem. Rev.* **2016**, *307*, 267–291. [CrossRef]

35. Chen, L.; Luque, R.; Li, Y. Controllable design of tunable nanostructures inside metal-organic framework. *Chem. Soc. Rev.* **2017**, *46*, 4614–4630. [CrossRef] [PubMed]

36. Xiao, J.D.; Shang, Q.; Xiong, Y.; Zhang, Q.; Luo, Y.; Yu, S.H.; Jiang, H.L. Boosting photocatalytic hydrogen production of a metal-organic framework decorated with platinum nanoparticles: The platinum location matters. *Angew. Chem. Int. Ed.* **2016**, *128*, 9535–9539. [CrossRef]

37. Vetter, S.; Haffer, S.; Wagner, T.; Tiemann, M. Nanostructured Co_3O_4 as a CO gas sensor: Temperature-dependent behavior. *Sens. Actuators B Chem.* **2015**, *206*, 133–138. [CrossRef]

38. Koop, J.; Deutschmann, O. Detailed surface reaction mechanism for Pt-catalyzed abatement of automotive exhaust gases. *Appl. Catal. B Environ.* **2009**, *91*, 47–58. [CrossRef]

39. Miao, Y.X.; Li, W.C.; Sun, Q.; Shi, L.; He, L.; Wang, J.; Deng, G.M.; Lu, A.H. Nanogold supported on manganese oxide doped alumina microspheres as a highly active and selective catalyst for CO oxidation in a H_2-rich stream. *Chem. Commun.* **2015**, *51*, 17728–17731. [CrossRef] [PubMed]

40. Zhou, Y.; Wang, Z.; Liu, C.J. Perspective on CO oxidation over Pd-based catalysts. *Catal. Sci. Technol.* **2015**, *5*, 69–81. [CrossRef]

41. Jiang, H.L.; Liu, B.; Akita, T.; Haruta, M.; Sakurai, H.; Xu, Q. Au@ ZIF-8: CO oxidation over gold nanoparticles deposited to metal−organic framework. *J. Am. Chem. Soc.* **2009**, *131*, 11302–11303. [CrossRef] [PubMed]

42. Ramos-Fernandez, E.V.; Pieters, C.; van der Linden, B.; Juan-Alcañiz, J.; Serra-Crespo, P.; Verhoeven, M.W.G.M.; Niemantsverdriet, H.; Gascon, J.; Kapteijn, F. Highly dispersed platinum in metal organic framework NH_2-MIL-101(Al) containing phosphotungstic acid–Characterization and catalytic performance. *J. Catal.* **2012**, *289*, 42–52. [CrossRef]

43. Wu, R.; Qian, X.; Zhou, K.; Liu, H.; Yadian, B.; Wei, J.; Zhu, H.; Huang, Y. Highly dispersed Au nanoparticles immobilized on Zr-based metal–organic frameworks as heterostructured catalyst for CO oxidation. *J. Mater. Chem. A* **2013**, *1*, 14294. [CrossRef]

44. Liang, Q.; Zhao, Z.; Liu, J.; Wei, Y.C.; Jiang, G.Y.; Duan, A.J. Pd Nanoparticles deposited on metal-organic framework of MIL-53 (Al) an active catalyst for CO oxidation. *Acta Phys.-Chim. Sin.* **2014**, *30*, 129–134. [CrossRef]

45. Zhuang, G.L.; Bai, J.Q.; Zhou, X.; Gao, Y.F.; Huang, H.L.; Cui, H.Q.; Zhong, X.; Zhong, C.L.; Wang, J.G. The Effect of N-Containing Supports on Catalytic CO Oxidation Activity over Highly Dispersed Pt/UiO-67. *Eur. J. Inorg. Chem.* **2017**, 172–178. [CrossRef]

46. Lin, A.; Ibrahim, A.A.; Arab, P.; El-Kaderi, H.M.; El-Shall, M.S. Palladium Nanoparticles Supported on Ce-Metal-Organic Framework for Efficient CO Oxidation and Low-Temperature CO_2 Capture. *ACS Appl. Mater. Interfaces* **2017**, *9*, 17961–17968. [CrossRef] [PubMed]

47. El-Shall, M.S.; Abdelsayed, V.; Khder, A.E.R.S.; Hassan, H.M.A.; El-Kaderi, H.M.; Reich, T.E. Metallic and bimetallic nanocatalysts incorporated into highly porous coordination polymer MIL-101. *J. Mater. Chem.* **2009**, *19*, 7625. [CrossRef]

48. Zhao, Y.; Zhong, C.; Liu, C.J. Enhanced CO oxidation over thermal treated Ag/Cu-BTC. *Catal. Commun.* **2013**, *38*, 74–76. [CrossRef]

49. Wang, W.; Li, Y.; Zhang, R.; He, D.; Liu, H.; Liao, S. Metal-organic framework as a host for synthesis of nanoscale Co_3O_4 as an active catalyst for CO oxidation. *Catal. Commun.* **2011**, *12*, 875–879. [CrossRef]

50. Shi, J.; Jiang, Y.; Jiang, Z.; Wang, X.; Wang, X.; Zhang, S.; Han, P.; Yang, C. Enzymatic conversion of carbon dioxide. *Chem. Soc. Rev.* **2015**, *44*, 5981–6000. [CrossRef] [PubMed]

51. Li, K.; Peng, B.; Peng, T. Recent Advances in Heterogeneous Photocatalytic CO_2 Conversion to Solar Fuels. *ACS Catal.* **2016**, *6*, 7485–7527. [CrossRef]

52. Zheng, Y.; Wang, J.; Yu, B.; Zhang, W.; Chen, J.; Qiao, J.; Zhang, J. A review of high temperature co-electrolysis of H_2O and CO_2 to produce sustainable fuels using solid oxide electrolysis cells (SOECs): Advanced materials and technology. *Chem. Soc. Rev.* **2017**, *46*, 1427–1463. [CrossRef] [PubMed]

53. Takeda, H.; Cometto, C.; Ishitani, O.; Robert, M. Electrons, photons, protons and earth-abundant metal complexes for molecular catalysis of CO_2 reduction. *ACS Catal.* **2017**, *7*, 70–88. [CrossRef]

54. Rungtaweevoranit, B.; Baek, J.; Araujo, J.R.; Archanjo, B.S.; Choi, K.M.; Yaghi, O.M.; Somorjai, G.A. Copper Nanocrystals Encapsulated in Zr-based Metal-Organic Frameworks for Highly Selective CO_2 Hydrogenation to Methanol. *Nano Lett.* **2016**, *16*, 7645–7649. [CrossRef] [PubMed]

55. An, B.; Zhang, J.; Cheng, K.; Ji, P.; Wang, C.; Lin, W. Confinement of Ultrasmall Cu/ZnO_x Nanoparticles in Metal-Organic Frameworks for Selective Methanol Synthesis from Catalytic Hydrogenation of CO_2. *J. Am. Chem. Soc.* **2017**, *139*, 3834–3840. [CrossRef] [PubMed]

56. Xu, H.; Li, Y.; Luo, X.; Xu, Z.; Ge, J. Monodispersed gold nanoparticles supported on a zirconium-based porous metal-organic framework and their high catalytic ability for the reverse water-gas shift reaction. *Chem. Commun.* **2017**, *53*, 7953–7956. [CrossRef] [PubMed]

57. Hu, S.; Liu, M.; Ding, F.; Song, C.; Zhang, G.; Guo, X. Hydrothermally stable MOFs for CO_2 hydrogenation over iron-based catalyst to light olefins. *J. CO_2 Util.* **2016**, *15*, 89–95. [CrossRef]

58. Crake, A.; Christoforidis, K.C.; Kafizas, A.; Zafeiratos, S.; Petit, C. CO_2 capture and photocatalytic reduction using bifunctional TiO_2/MOF nanocomposites under UV-vis irradiation. *Appl. Catal. B Environ.* **2017**, *210*, 131–140. [CrossRef]

59. Li, R.; Hu, J.; Deng, M.; Wang, H.; Wang, X.; Hu, Y.; Jiang, H.L.; Jiang, J.; Zhang, Q.; Xie, Y.; Xiong, Y. Integration of an inorganic semiconductor with a metal-organic framework: A platform for enhanced gaseous photocatalytic reactions. *Adv. Mater.* **2014**, *26*, 4783–4788. [CrossRef] [PubMed]

60. Wang, M.; Wang, D.; Li, Z. Self-assembly of $CPO-27-Mg/TiO_2$ nanocomposite with enhanced performance for photocatalytic CO_2 reduction. *Appl. Catal. B Environ.* **2016**, *183*, 47–52. [CrossRef]

61. Wang, S.; Wang, X. Photocatalytic CO_2 reduction by CdS promoted with a zeolitic imidazolate framework. *Appl. Catal. B Environ.* **2015**, *162*, 494–500. [CrossRef]

62. Liu, Q.; Low, Z.X.; Li, L.; Razmjou, A.; Wang, K.; Yao, J.; Wang, H. $ZIF-8/Zn_2GeO_4$ nanorods with an enhanced CO_2 adsorption property in an aqueous medium for photocatalytic synthesis of liquid fuel. *J. Mater. Chem. A* **2013**, *1*, 11563. [CrossRef]

63. Liu, S.; Chen, F.; Li, S.; Peng, X.; Xiong, Y. Enhanced photocatalytic conversion of greenhouse gas CO_2 into solar fuels over $g-C_3N_4$ nanotubes with decorated transparent ZIF-8 nanoclusters. *Appl. Catal. B Environ.* **2017**, *211*, 1–10. [CrossRef]

64. Choi, K.M.; Kim, D.; Rungtaweevoranit, B.; Trickett, C.A.; Barmanbek, J.T.; Alshammari, A.S.; Yang, P.; Yaghi, O.M. Plasmon-Enhanced Photocatalytic CO_2 Conversion within Metal-Organic Frameworks under Visible Light. *J. Am. Chem. Soc.* **2017**, *139*, 356–362. [CrossRef] [PubMed]

65. Su, Y.; Zhang, Z.; Liu, H.; Wang, Y. $Cd_{0.2}Zn_{0.8}S@UiO-66-NH_2$ nanocomposites as efficient and stable visible-light-driven photocatalyst for H 2 evolution and CO_2 reduction. *Appl. Catal. B Environ.* **2017**, *200*, 448–457. [CrossRef]

66. Wang, W.; Xu, X.; Zhou, W.; Shao, Z. Recent Progress in Metal-Organic Frameworks for Applications in Electrocatalytic and Photocatalytic Water Splitting. *Adv. Sci.* **2017**, *4*, 1600371. [CrossRef] [PubMed]

67. Xu, B.H.; Wang, J.Q.; Sun, J.; Huang, Y.; Zhang, J.P.; Zhang, X.P.; Zhang, S.J. Fixation of CO_2 into cyclic carbonates catalyzed by ionic liquids: A multi-scale approach. *Green Chem.* **2015**, *17*, 108–122. [CrossRef]

68. Sołtys-Brzostek, K.; Terlecki, M.; Sokołowski, K.; Lewiński, J. Chemical fixation and conversion of CO_2 into cyclic and cage-type metal carbonates. *Coord. Chem. Rev.* **2017**, *334*, 199–231. [CrossRef]

69. Luo, Q.X.; Ji, M.; Lu, M.H.; Hao, C.; Qiu, J.S.; Li, Y.Q. Organic electron-rich N-heterocyclic compound as a chemical bridge: Building a Brönsted acidic ionic liquid confined in MIL-101 nanocages. *J. Mater. Chem. A* **2013**, *1*, 6530–6534. [CrossRef]

70. Liang, J.; Chen, R.P.; Wang, X.Y.; Liu, T.T.; Wang, X.S.; Huang, Y.B.; Cao, R. Postsynthetic ionization of an imidazole-containing metal–organic framework for the cycloaddition of carbon dioxide and epoxides. *Chem. Sci.* **2017**, *8*, 1570–1575. [CrossRef] [PubMed]

71. Ding, L.G.; Yao, B.J.; Jiang, W.L.; Li, J.T.; Fu, Q.J.; Li, Y.A.; Liu, Z.H.; Ma, J.P.; Dong, Y.B. Bifunctional Imidazolium-Based Ionic Liquid Decorated UiO-67 Type MOF for Selective CO_2 Adsorption and Catalytic Property for CO_2 Cycloaddition with Epoxides. *Inorg. Chem.* **2017**, *56*, 2337–2344. [CrossRef] [PubMed]

72. Ma, D.; Li, B.; Liu, K.; Zhang, X.; Zou, W.; Yang, Y.; Li, G.; Shi, Z.; Feng, S. Bifunctional MOF heterogeneous catalysts based on the synergy of dual functional sites for efficient conversion of CO_2 under mild and co-catalyst free conditions. *J. Mater. Chem. A* **2015**, *3*, 23136–23142. [CrossRef]

73. Tharun, J.; Bhin, K.M.; Roshan, R.; Kim, D.W.; Kathalikkattil, A.C.; Babu, R.; Ahn, H.Y.; Won, Y.S.; Park, D.W. Ionic liquid tethered post functionalized ZIF-90 framework for the cycloaddition of propylene oxide and CO$_2$. *Green Chem.* **2016**, *18*, 2479–2487. [CrossRef]

74. Gu, X.; Lu, Z.H.; Jiang, H.L.; Akita, T.; Xu, Q. Synergistic catalysis of metal-organic framework-immobilized Au-Pd nanoparticles in dehydrogenation of formic acid for chemical hydrogen storage. *J. Am. Chem. Soc.* **2011**, *133*, 11822–11825. [CrossRef] [PubMed]

75. Li, P.Z.; Aranishi, K.; Xu, Q. ZIF-8 immobilized nickel nanoparticles: Highly effective catalysts for hydrogen generation from hydrolysis of ammonia borane. *Chem. Commun.* **2012**, *48*, 3173–3175. [CrossRef] [PubMed]

76. Singh, A.K.; Xu, Q. Metal-Organic Framework Supported Bimetallic Ni@Pt Nanoparticles as High-performance Catalysts for Hydrogen Generation from Hydrazine in Aqueous Solution. *ChemCatChem* **2013**, *5*, 3000–3004. [CrossRef]

77. Cao, N.; Liu, T.; Su, J.; Wu, X.; Luo, W.; Cheng, G. Ruthenium supported on MIL-101 as an efficient catalyst for hydrogen generation from hydrolysis of amine boranes. *New J. Chem.* **2014**, *38*, 4032. [CrossRef]

78. Cao, N.; Yang, L.; Dai, H.; Liu, T.; Su, J.; Wu, X.; Luo, W.; Cheng, G. Immobilization of ultrafine bimetallic Ni-Pt nanoparticles inside the pores of metal-organic frameworks as efficient catalysts for dehydrogenation of alkaline solution of hydrazine. *Inorg. Chem.* **2014**, *53*, 10122–10128. [CrossRef] [PubMed]

79. Dai, H.; Cao, N.; Yang, L.; Su, J.; Luo, W.; Cheng, G. AgPd nanoparticles supported on MIL-101 as high performance catalysts for catalytic dehydrogenation of formic acid. *J. Mater. Chem. A* **2014**, *2*, 11060. [CrossRef]

80. Xia, B.; Cao, N.; Dai, H.; Su, J.; Wu, X.; Luo, W.; Cheng, G. Bimetallic Nickel-Rhodium Nanoparticles Supported on ZIF-8 as Highly Efficient Catalysts for Hydrogen Generation from Hydrazine in Alkaline Solution. *ChemCatChem* **2014**, *6*, 2549–2552. [CrossRef]

81. Chen, Y.Z.; Xu, Q.; Yu, S.H.; Jiang, H.L. Tiny Pd@Co core-shell nanoparticles confined inside a metal-organic framework for highly efficient catalysis. *Small* **2015**, *11*, 71–76. [CrossRef] [PubMed]

82. Dai, H.; Xia, B.; Wen, L.; Du, C.; Su, J.; Luo, W.; Cheng, G. Synergistic catalysis of AgPd@ZIF-8 on dehydrogenation of formic acid. *Appl. Catal. B Environ.* **2015**, *165*, 57–62. [CrossRef]

83. Ke, F.; Wang, L.; Zhu, J. An efficient room temperature core-shell AgPd@MOF catalyst for hydrogen production from formic acid. *Nanoscale* **2015**, *7*, 8321–8325. [CrossRef] [PubMed]

84. Zhao, P.; Cao, N.; Luo, W.; Cheng, G. Nanoscale MIL-101 supported RhNi nanoparticles: An efficient catalyst for hydrogen generation from hydrous hydrazine. *J. Mater. Chem. A* **2015**, *3*, 12468–12475. [CrossRef]

85. Zhao, P.; Cao, N.; Su, J.; Luo, W.; Cheng, G. NiIr Nanoparticles Immobilized on the Pores of MIL-101 as Highly Efficient Catalyst toward Hydrogen Generation from Hydrous Hydrazine. *ACS Sustain. Chem. Eng.* **2015**, *3*, 1086–1093. [CrossRef]

86. Cheng, J.; Gu, X.; Liu, P.; Wang, T.; Su, H. Controlling catalytic dehydrogenation of formic acid over low-cost transition metal-substituted AuPd nanoparticles immobilized by functionalized metal–organic frameworks at room temperature. *J. Mater. Chem. A* **2016**, *4*, 16645–16652. [CrossRef]

87. Gao, S.T.; Liu, W.; Feng, C.; Shang, N.Z.; Wang, C. A Ag-Pd alloy supported on an amine-functionalized UiO-66 as an efficient synergetic catalyst for the dehydrogenation of formic acid at room temperature. *Catal. Sci. Technol.* **2016**, *6*, 869–874. [CrossRef]

88. Wen, M.; Cui, Y.; Kuwahara, Y.; Mori, K.; Yamashita, H. Non-Noble-Metal Nanoparticle Supported on Metal-Organic Framework as an Efficient and Durable Catalyst for Promoting H$_2$ Production from Ammonia Borane under Visible Light Irradiation. *ACS Appl. Mater. Interfaces* **2016**, *8*, 21278–21284. [CrossRef] [PubMed]

89. Wen, M.; Kuwahara, Y.; Mori, K.; Yamashita, H. Enhancement of Catalytic Activity Over AuPd Nanoparticles Loaded Metal Organic Framework under Visible Light Irradiation. *Top. Catal.* **2016**, *59*, 1765–1771. [CrossRef]

90. Liu, P.; Gu, X.; Kang, K.; Zhang, H.; Cheng, J.; Su, H. Highly Efficient Catalytic Hydrogen Evolution from Ammonia Borane Using the Synergistic Effect of Crystallinity and Size of Noble-Metal-Free Nanoparticles Supported by Porous Metal-Organic Frameworks. *ACS Appl. Mater. Interfaces* **2017**, *9*, 10759–10767. [CrossRef] [PubMed]

91. Wen, M.; Mori, K.; Kuwahara, Y.; Yamashita, H. Plasmonic Au@Pd Nanoparticles Supported on a Basic Metal–Organic Framework: Synergic Boosting of H$_2$ Production from Formic Acid. *ACS Energy Lett.* **2017**, *2*, 1–7. [CrossRef]

92. Toyao, T.; Saito, M.; Horiuchi, Y.; Mochizuki, K.; Iwata, M.; Higashimura, H.; Matsuoka, M. Efficient hydrogen production and photocatalytic reduction of nitrobenzene over a visible-light-responsive metal–organic framework photocatalyst. *Catal. Sci. Technol.* **2013**, *3*, 2092. [CrossRef]

93. Wen, M.; Mori, K.; Kamegawa, T.; Yamashita, H. Amine-functionalized MIL-101(Cr) with imbedded platinum nanoparticles as a durable photocatalyst for hydrogen production from water. *Chem. Commun.* **2014**, *50*, 11645–11648. [CrossRef] [PubMed]

94. Zhen, W.; Ma, J.; Lu, G. Small-sized Ni(1 1 1) particles in metal-organic frameworks with low over-potential for visible photocatalytic hydrogen generation. *Appl. Catal. B Environ.* **2016**, *190*, 12–25. [CrossRef]

95. He, J.; Yan, Z.; Wang, J.; Xie, J.; Jiang, L.; Shi, Y.; Yuan, F.; Yu, F.; Sun, Y. Significantly enhanced photocatalytic hydrogen evolution under visible light over CdS embedded on metal-organic frameworks. *Chem. Commun.* **2013**, *49*, 6761–6763. [CrossRef] [PubMed]

96. Shen, L.; Luo, M.; Liu, Y.; Liang, R.; Jing, F.; Wu, L. Noble-metal-free MoS_2 co-catalyst decorated UiO-66/CdS hybrids for efficient photocatalytic H2 production. *Appl. Catal. B Environ.* **2015**, *166–167*, 445–453. [CrossRef]

97. Peters, A.W.; Li, Z.; Farha, O.K.; Hupp, J.T. Toward Inexpensive Photocatalytic Hydrogen Evolution: A Nickel Sulfide Catalyst Supported on a High-Stability Metal-Organic Framework. *ACS Appl. Mater. Interfaces* **2016**, *8*, 20675–20681. [CrossRef] [PubMed]

98. Hao, X.; Jin, Z.; Yang, H.; Lu, G.; Bi, Y. Peculiar synergetic effect of MoS_2 quantum dots and graphene on Metal-Organic Frameworks for photocatalytic hydrogen evolution. *Appl. Catal. B Environ.* **2017**, *210*, 45–56. [CrossRef]

99. Lin, R.; Shen, L.; Ren, Z.; Wu, W.; Tan, Y.; Fu, H.; Zhang, J.; Wu, L. Enhanced photocatalytic hydrogen production activity via dual modification of MOF and reduced graphene oxide on CdS. *Chem. Commun.* **2014**, *50*, 8533–8535. [CrossRef] [PubMed]

100. Wang, R.; Gu, L.; Zhou, J.; Liu, X.; Teng, F.; Li, C.; Shen, Y.; Yuan, Y. Quasi-Polymeric Metal-Organic Framework UiO-66/g-C_3N_4 Heterojunctions for Enhanced Photocatalytic Hydrogen Evolution under Visible Light Irradiation. *Adv. Mater. Interfaces* **2015**, *2*, 1500037. [CrossRef]

101. Kong, X.J.; Lin, Z.; Zhang, Z.M.; Zhang, T.; Lin, W. Hierarchical Integration of Photosensitizing Metal-Organic Framework and Nickel-Containing Polyoxometalates for Efficient Visible-Light Driven Hydrogen Evolution. *Angew. Chem. Int. Ed.* **2016**, *55*, 6411–6416. [CrossRef] [PubMed]

102. Liu, H.; Liu, Y.; Li, Y.; Tang, Z.; Jiang, H. Metal−organic framework supported gold nanoparticles as a highly active heterogeneous catalyst for aerobic oxidation of alcohols. *J. Phys. Chem. C* **2010**, *114*, 13362–13369. [CrossRef]

103. Chen, L.; Chen, H.; Luque, R.; Li, Y. Metal−organic framework encapsulated Pd nanoparticles: Towards advanced heterogeneous catalysts. *Chem. Sci.* **2014**, *5*, 3708–3714. [CrossRef]

104. Liu, H.; Chang, L.; Chen, L.; Li, Y. In situ one-step synthesis of metal–organic framework encapsulated naked Pt nanoparticles without additional reductants. *J. Mater. Chem. A* **2015**, *3*, 8028–8033. [CrossRef]

105. Shen, L.; Liang, S.; Wu, W.; Liang, R.; Wu, L. CdS-decorated UiO–66(NH_2) nanocomposites fabricated by a facile photodeposition process: An efficient and stable visible-light-driven photocatalyst for selective oxidation of alcohols. *J. Mater. Chem. A* **2013**, *1*, 11473. [CrossRef]

106. Liu, L.; Song, Y.; Chong, H.; Yang, S.; Xiang, J.; Jin, S.; Kang, X.; Zhang, J.; Yu, H.; Zhu, M. Size-confined growth of atom-precise nanoclusters in metal-organic frameworks and their catalytic applications. *Nanoscale* **2016**, *8*, 1407–1412. [CrossRef] [PubMed]

107. Cai, J.; Lu, J.Y.; Chen, Q.Y.; Qu, L.L.; Lu, Y.Q.; Gao, G.F. Eu-Based MOF/graphene oxide composite: A novel photocatalyst for the oxidation of benzyl alcohol using water as oxygen source. *New J. Chem.* **2017**, *41*, 3882–3886. [CrossRef]

108. Qiu, X.; Wang, X.; Li, Y. Controlled growth of dense and ordered metal-organic framework nanoparticles on graphene oxide. *Chem. Commun.* **2015**, *51*, 3874–3877. [CrossRef] [PubMed]

109. Zhu, J.; Shen, M.N.; Zhao, X.J.; Wang, P.C.; Lu, M. Polyoxometalate-Based Metal-Organic Frameworks as Catalysts for the Selective Oxidation of Alcohols in Micellar Systems. *ChemPlusChem* **2014**, *79*, 872–878. [CrossRef]

110. Luan, Y.; Qi, Y.; Gao, H.; Zheng, N.; Wang, G. Synthesis of an amino-functionalized metal–organic framework at a nanoscale level for gold nanoparticle deposition and catalysis. *J. Mater. Chem. A* **2014**, *2*, 20588–20596. [CrossRef]

111. Verma, S.; Baig, R.B.; Nadagouda, M.N.; Varma, R.S. Aerobic oxidation of alcohols in visible light on Pd-grafted Ti cluster. *Tetrahedron* **2017**, *73*, 5577–5580. [CrossRef]

112. Sun, Z.; Li, G.; Liu, L.; Liu, H.O. Au nanoparticles supported on Cr-based metal-organic framework as bimetallic catalyst for selective oxidation of cyclohexane to cyclohexanone and cyclohexanol. *Catal. Commun.* **2012**, *27*, 200–205. [CrossRef]

113. Long, J.; Liu, H.; Wu, S.; Liao, S.; Li, Y. Selective Oxidation of Saturated Hydrocarbons Using Au–Pd Alloy Nanoparticles Supported on Metal–Organic Frameworks. *ACS Catal.* **2013**, *3*, 647–654. [CrossRef]

114. Huang, Y.; Zhang, Y.; Chen, X.; Wu, D.; Yi, Z.; Cao, R. Bimetallic alloy nanocrystals encapsulated in ZIF-8 for synergistic catalysis of ethylene oxidative degradation. *Chem. Commun.* **2014**, *50*, 10115–10117. [CrossRef] [PubMed]

115. Granadeiro, C.M.; Barbosa, A.D.; Silva, P.; Paz, F.A.A.; Saini, V.K.; Pires, J.; Castro, B.; Balula, S.S.; Cunha-Silva, L. Monovacant polyoxometalates incorporated into MIL-101 (Cr): Novel heterogeneous catalysts for liquid phase oxidation. *Appl. Catal. A: Gen.* **2013**, *453*, 316–326. [CrossRef]

116. Tong, J.; Wang, W.; Su, L.; Li, Q.; Liu, F.; Ma, W.; Lei, Z.; Bo, L. Highly selective oxidation of cyclohexene to 2-cyclohexene-1-one over polyoxometalate/metal-organic framework hybrids with greatly improved performance. *Catal. Sci. Technol.* **2017**, *7*, 222–230. [CrossRef]

117. Aguado, S.; El-Jamal, S.; Meunier, F.; Canivet, J.; Farrusseng, D. A Pt/Al$_2$O$_3$-supported metal-organic framework film as the size-selective core-shell hydrogenation catalyst. *Chem. Commun.* **2016**, *52*, 7161–7163. [CrossRef] [PubMed]

118. Jia, X.; Wang, S.; Fan, Y. A novel strategy for producing highly dispersed Pd particles on ZIF-8 through the occupation and unoccupation of carboxyl groups and its application in selective diene hydrogenation. *J. Catal.* **2015**, *327*, 54–57. [CrossRef]

119. Zhang, W.; Lu, G.; Cui, C.; Liu, Y.; Li, S.; Yan, W.; Xing, C.; Chi, Y.R.; Yang, Y.; Huo, F. A family of metal-organic frameworks exhibiting size-selective catalysis with encapsulated noble-metal nanoparticles. *Adv. Mater.* **2014**, *26*, 4056–4060. [CrossRef] [PubMed]

120. Liu, Y.; Zhang, W.; Li, S.; Cui, C.; Wu, J.; Chen, H.; Huo, F. Designable Yolk–Shell Nanoparticle@MOF Petalous Heterostructures. *Chem. Mater.* **2014**, *26*, 1119–1125. [CrossRef]

121. Chen, L.; Li, H.; Zhan, W.; Cao, Z.; Chen, J.; Jiang, Q.; Jiang, Y.; Xie, Z.; Kuang, Q.; Zheng, L. Controlled Encapsulation of Flower-like Rh-Ni Alloys with MOFs via Tunable Template Dealloying for Enhanced Selective Hydrogenation of Alkyne. *ACS Appl. Mater. Interfaces* **2016**, *8*, 31059–31066. [CrossRef] [PubMed]

122. Chen, L.; Huang, B.; Qiu, X.; Wang, X.; Luque, R.; Li, Y. Seed-mediated growth of MOF-encapsulated Pd@Ag core-shell nanoparticles: Toward advanced room temperature nanocatalysts. *Chem. Sci.* **2016**, *7*, 228–233. [CrossRef] [PubMed]

123. Bi, H.; Tan, X.; Dou, R.; Pei, Y.; Qiao, M.; Sun, B.; Zong, B. Ru–B nanoparticles on metal–organic frameworks as excellent catalysts for hydrogenation of benzene to cyclohexane under mild reaction conditions. *Green Chem.* **2016**, *18*, 2216–2221. [CrossRef]

124. Chen, L.; Huang, W.; Wang, X.; Chen, Z.; Yang, X.; Luque, R.; Li, Y. Catalytically active designer crown-jewel Pd-based nanostructures encapsulated in metal-organic frameworks. *Chem. Commun.* **2017**, *53*, 1184–1187. [CrossRef] [PubMed]

125. Chen, L.Y.; Chen, X.D.; Liu, H.L.; Li, Y.W. Encapsulation of Mono- or Bimetal Nanoparticles Inside Metal-Organic Frameworks via In situ Incorporation of Metal Precursors. *Small* **2015**, *11*, 2642–2648. [CrossRef] [PubMed]

126. Hermannsdorfer, J.; Friedrich, M.; Miyajima, N.; Albuquerque, R.Q.; Kummel, S.; Kempe, R. Ni/Pd@MIL-101: Synergistic catalysis with cavity-conform Ni/Pd nanoparticles. *Angew. Chem. Int. Ed.* **2012**, *51*, 11473–11477. [CrossRef] [PubMed]

127. Lan, X.; Huang, N.; Wang, J.; Wang, T. Geometric effect in the highly selective hydrogenation of 3-methylcrotonaldehyde over Pt@ZIF-8 core–shell catalysts. *Catal. Sci. Technol.* **2017**, *7*, 2601–2608. [CrossRef]

128. Zhao, M.; Yuan, K.; Wang, Y.; Li, G.; Guo, J.; Gu, L.; Hu, W.; Zhao, H.; Tang, Z. Metal-organic frameworks as selectivity regulators for hydrogenation reactions. *Nature* **2016**, *539*, 76–80. [CrossRef] [PubMed]

129. Stavila, V.; Parthasarathi, R.; Davis, R.W.; El Gabaly, F.; Sale, K.L.; Simmons, B.A.; Singh, S.; Allendorf, M.D. MOF-Based Catalysts for Selective Hydrogenolysis of Carbon–Oxygen Ether Bonds. *ACS Catal.* **2015**, *6*, 55–59. [CrossRef]

130. Aijaz, A.; Zhu, Q.L.; Tsumori, N.; Akita, T.; Xu, Q. Surfactant-free Pd nanoparticles immobilized to a metal-organic framework with size- and location-dependent catalytic selectivity. *Chem. Commun.* **2015**, *51*, 2577–2580. [CrossRef] [PubMed]

131. Lu, G.; Li, S.; Guo, Z.; Farha, O.K.; Hauser, B.G.; Qi, X.; Wang, Y.; Wang, X.; Han, S.; Liu, X. Imparting functionality to a metal–organic framework material by controlled nanoparticle encapsulation. *Nat. Chem.* **2012**, *4*, 310–316. [CrossRef] [PubMed]

132. Wang, P.; Zhao, J.; Li, X.; Yang, Y.; Yang, Q.; Li, C. Assembly of ZIF nanostructures around free Pt nanoparticles: Efficient size-selective catalysts for hydrogenation of alkenes under mild conditions. *Chem. Commun.* **2013**, *49*, 3330–3332. [CrossRef] [PubMed]

133. Roy, A.S.; Mondal, J.; Banerjee, B.; Mondal, P.; Bhaumik, A.; Islam, S.M. Pd-grafted porous metal–organic framework material as an efficient and reusable heterogeneous catalyst for C–C coupling reactions in water. *Appl. Catal. A Gen.* **2014**, *469*, 320–327. [CrossRef]

134. Pourkhosravani, M.; Dehghanpour, S.; Farzaneh, F. Palladium Nanoparticles Supported on Zirconium Metal Organic Framework as an Efficient Heterogeneous Catalyst for the Suzuki–Miyaura Coupling Reaction. *Catal. Lett.* **2015**, *146*, 499–508. [CrossRef]

135. Sun, D.; Li, Z. Double-Solvent Method to Pd Nanoclusters Encapsulated inside the Cavity of NH_2–Uio-66(Zr) for Efficient Visible-Light-Promoted Suzuki Coupling Reaction. *J. Phys. Chem. C* **2016**, *120*, 19744–19750. [CrossRef]

136. Yang, Y.; Cong, D.; Hao, S. Template-Directed Ordered Mesoporous Silica@Palladium-Containing Zinc Metal-Organic Framework Composites as Highly Efficient Suzuki Coupling Catalysts. *ChemCatChem* **2016**, *8*, 900–905. [CrossRef]

137. Augustyniak, A.W.; Zawartka, W.; Navarro, J.A.; Trzeciak, A.M. Palladium nanoparticles supported on a nickel pyrazolate metal organic framework as a catalyst for Suzuki and carbonylative Suzuki couplings. *Dalton Trans.* **2016**, *45*, 13525–13531. [CrossRef] [PubMed]

138. Liang, R.; Shen, L.; Jing, F.; Qin, N.; Wu, L. Preparation of MIL-53(Fe)-Reduced Graphene Oxide Nanocomposites by a Simple Self-Assembly Strategy for Increasing Interfacial Contact: Efficient Visible-Light Photocatalysts. *ACS Appl. Mater. Interfaces* **2015**, *7*, 9507–9515. [CrossRef] [PubMed]

139. Wang, X.B.; Liu, J.; Leong, S.; Lin, X.C.; Wei, J.; Kong, B.; Xu, Y.F.; Low, Z.X.; Yao, J.F.; Wang, H.T. Rapid Construction of ZnO@ZIF-8 Heterostructures with Size-Selective Photocatalysis Properties. *ACS Appl. Mater. Interfaces* **2016**, *8*, 9080–9087. [CrossRef] [PubMed]

140. Araya, T.; Jia, M.; Yang, J.; Zhao, P.; Cai, K.; Ma, W.; Huang, Y. Resin modified MIL-53 (Fe) MOF for improvement of photocatalytic performance. *Appl. Catal. B Environ.* **2017**, *203*, 768–777. [CrossRef]

141. Wang, H.; Yuan, X.; Wu, Y.; Zeng, G.; Chen, X.; Leng, L.; Li, H. Synthesis and applications of novel graphitic carbon nitride/metal-organic frameworks mesoporous photocatalyst for dyes removal. *Appl. Catal. B Environ.* **2015**, *174–175*, 445–454. [CrossRef]

142. Wang, H.; Yuan, X.; Wu, Y.; Zeng, G.; Dong, H.; Chen, X.; Leng, L.; Wu, Z.; Peng, L. In situ synthesis of In_2S_3@MIL-125(Ti) core–shell microparticle for the removal of tetracycline from wastewater by integrated adsorption and visible-light-driven photocatalysis. *Appl. Catal. B Environ.* **2016**, *186*, 19–29. [CrossRef]

143. Hu, L.; Deng, G.; Lu, W.; Pang, S.; Hu, X. Deposition of CdS nanoparticles on MIL-53(Fe) metal-organic framework with enhanced photocatalytic degradation of RhB under visible light irradiation. *Appl. Surf. Sci.* **2017**, *410*, 401–413. [CrossRef]

144. Hong, J.; Chen, C.; Bedoya, F.E.; Kelsall, G.H.; O'Hare, D.; Petit, C. Carbon nitride nanosheet/metal–organic framework nanocomposites with synergistic photocatalytic activities. *Catal. Sci. Technol.* **2016**, *6*, 5042–5051. [CrossRef]

145. Yadav, M.; Xu, Q. Catalytic chromium reduction using formic acid and metal nanoparticles immobilized in a metal-organic framework. *Chem. Commun.* **2013**, *49*, 3327–3329. [CrossRef] [PubMed]

146. Kaur, R.; Vellingiri, K.; Kim, K.H.; Paul, A.K.; Deep, A. Efficient photocatalytic degradation of rhodamine 6G with a quantum dot-metal organic framework nanocomposite. *Chemosphere* **2016**, *154*, 620–627. [CrossRef] [PubMed]

147. Zhu, S.R.; Wu, M.K.; Zhao, W.N.; Liu, P.F.; Yi, F.Y.; Li, G.C.; Tao, K.; Han, L. In Situ Growth of Metal–Organic Framework on BiOBr 2D Material with Excellent Photocatalytic Activity for Dye Degradation. *Cryst. Growth Des.* **2017**, *17*, 2309–2313. [CrossRef]

148. Jahurul Islam, M.; Kim, H.K.; Amaranatha Reddy, D.; Kim, Y.; Ma, R.; Baek, H.; Kim, J.; Kim, T.K. Hierarchical BiOI nanostructures supported on a metal organic framework as efficient photocatalysts for degradation of organic pollutants in water. *Dalton Trans.* **2017**, *46*, 6013–6023. [CrossRef] [PubMed]

149. Zhu, S.R.; Liu, P.F.; Wu, M.K.; Zhao, W.N.; Li, G.C.; Tao, K.; Yi, F.Y.; Han, L. Enhanced photocatalytic performance of BiOBr/NH$_2$-MIL-125(Ti) composite for dye degradation under visible light. *Dalton Trans.* **2016**, *45*, 17521–17529. [CrossRef] [PubMed]

150. Zeng, T.; Zhang, X.; Wang, S.; Niu, H.; Cai, Y. Spatial confinement of a Co$_3$O$_4$ catalyst in hollow metal-organic frameworks as a nanoreactor for improved degradation of organic pollutants. *Environ. Sci. Technol.* **2015**, *49*, 2350–2357. [CrossRef] [PubMed]

151. Hu, Y.; Huang, Z.; Zhou, L.; Wang, D.; Li, G. Synthesis of nanoscale titania embedded in MIL-101 for the adsorption and degradation of volatile pollutants with thermal desorption gas chromatography and mass spectrometry detection. *J. Sep. Sci.* **2014**, *37*, 1482–1488. [CrossRef] [PubMed]

152. Li, H.C.; Liu, W.J.; Han, H.X.; Yu, H.Q. Hydrophilic swellable metal–organic framework encapsulated Pd nanoparticles as an efficient catalyst for Cr(VI) reduction. *J. Mater. Chem. A* **2016**, *4*, 11680–11687. [CrossRef]

153. Cheng, C.; Fang, J.; Lu, S.; Cen, C.; Chen, Y.; Ren, L.; Feng, W.; Fang, Z. Zirconium metal-organic framework supported highly-dispersed nanosized BiVO4for enhanced visible-light photocatalytic applications. *J. Chem. Technol. Biotechnol.* **2016**, *91*, 2785–2792. [CrossRef]

154. Zhang, C.F.; Qiu, L.G.; Ke, F.; Zhu, Y.J.; Yuan, Y.P.; Xu, G.S.; Jiang, X. A novel magnetic recyclable photocatalyst based on a core–shell metal–organic framework Fe$_3$O$_4$@MIL-100(Fe) for the decolorization of methylene blue dye. *J. Mater. Chem. A* **2013**, *1*, 14329. [CrossRef]

155. Shen, L.; Wu, W.; Liang, R.; Lin, R.; Wu, L. Highly dispersed palladium nanoparticles anchored on UiO-66(NH$_2$)) metal-organic framework as a reusable and dual functional visible-light-driven photocatalyst. *Nanoscale* **2013**, *5*, 9374–9382. [CrossRef] [PubMed]

156. Wee, L.H.; Janssens, N.; Sree, S.P.; Wiktor, C.; Gobechiya, E.; Fischer, R.A.; Kirschhock, C.E.; Martens, J.A. Local transformation of ZIF-8 powders and coatings into ZnO nanorods for photocatalytic application. *Nanoscale* **2014**, *6*, 2056–2060. [CrossRef] [PubMed]

157. Trivedi, M.; Bhaskaran, B.; Kumar, A.; Singh, G.; Kumar, A.; Rath, N.P. Metal-organic framework MIL-101 supported bimetallic Pd–Cu nanocrystals as efficient catalysts for chromium reduction and conversion of carbon dioxide at room temperature. *New J. Chem.* **2016**, *40*, 3109–3118. [CrossRef]

158. Sha, Z.; Wu, J. Enhanced visible-light photocatalytic performance of BiOBr/UiO-66(Zr) composite for dye degradation with the assistance of UiO-66. *RSC Adv.* **2015**, *5*, 39592–39600. [CrossRef]

159. Shen, L.; Huang, L.; Liang, S.; Liang, R.; Qin, N.; Wu, L. Electrostatically derived self-assembly of NH$_2$-mediated zirconium MOFs with graphene for photocatalytic reduction of Cr(vi). *RSC Adv.* **2014**, *4*, 2546–2549. [CrossRef]

160. Wang, C.C.; Li, J.R.; Lv, X.L.; Zhang, Y.Q.; Guo, G. Photocatalytic organic pollutants degradation in metal-organic frameworks. *Energy Environ. Sci.* **2014**, *7*, 2831–2867. [CrossRef]

161. Zhang, M.H.; Huang, X.W.; Chen, Y.F. DFT insights into the adsorption of NH$_3$-SCR related small gases in Mn-MOF-74. *Phys. Chem. Chem. Phys.* **2016**, *18*, 28854–28863. [CrossRef] [PubMed]

162. Ye, J.; Johnson, J.K. Screening Lewis pair moieties for catalytic hydrogenation of CO$_2$ in functionalized UiO-66. *ACS Catal.* **2015**, *5*, 6219–6229. [CrossRef]

163. Rui, N.; Wang, Z.; Sun, K.; Ye, J.; Ge, Q.; Liu, C.-J. CO$_2$ hydrogenation to methanol over Pd/In$_2$O$_3$: Effects of Pd and oxygen vacancy. *Appl. Catal. B Environ.* **2017**, *218*, 488–497. [CrossRef]

164. Wang, W.; Anderson, C.; Wang, Z.; Wu, W.; Cui, H.; Liu, C.-J. Peptide-templated noble metal catalysts: Syntheses and applications. *Chem. Sci.* **2017**, *8*, 3310–3324. [CrossRef] [PubMed]

165. Wang, W.; Wang, Z.; Yang, M.; Zhong, C.-J.; Liu, C.-J. Highly active and stable Pt (111) catalysts synthesized by peptide Assisted room temperature electron reduction for oxygen reduction reaction. *Nano Energy* **2016**, *25*, 26–33. [CrossRef]

166. Wang, W.; Wang, Z.; Wang, J.; Zhong, C.-J.; Liu, C.-J. Highly active and stable Pt-Pd alloy catalysts synthesized by room temperature electron reduction for oxygen reduction reaction. *Adv. Sci.* **2017**, *4*, 1600486. [CrossRef] [PubMed]

167. Liu, C.-J.; Li, M.; Wang, J.; Zhou, X.; Guo, Q.; Yan, J.; Li, Y. Cold plasma applications for green catalyst preparation: Current status and perspective. *Chin. J. Catal.* **2016**, *37*, 340–348. [CrossRef]

168. Qin, L.; Li, Z.; Hu, Q.; Xu, Z.; Guo, X.; Zhang, G. One-pot assembly of metal/organic-acid sites on amine-functionalized ligands of MOFs for photocatalytic hydrogen peroxide splitting. *Chem. Commun.* **2016**, *52*, 7110–7113. [CrossRef] [PubMed]

169. Li, W.; Su, P.; Li, Z.; Xu, Z.; Wang, F.; Ou, H.; Zhang, J.; Zhang, G.; Zeng, E. Ultrathin metal–organic framework membrane production by gel–vapour deposition. *Nat. Commun.* **2017**, *8*, 406. [CrossRef] [PubMed]

170. Zhu, L.; Liu, X.-Q.; Jiang, H.-L.; Sun, L.-B. Metal−organic frameworks for heterogeneous basic catalysis. *Chem. Rev.* **2017**, *117*, 8129–8176. [CrossRef] [PubMed]

171. Metzger, E.D.; Comito, R.J.; Hendon, C.H.; Dinca, M. Mechanism of single-site molecule-like catalytic ethylene dimerization in Ni-MFU-4l. *J. Am. Chem. Soc.* **2017**, *139*, 757–762. [CrossRef] [PubMed]

172. Chaemchuen, S.; Luo, Z.; Zhou, K.; Mousavi, B.; Phatanasri, S.; Jaroniec, M.; Verpoort, F. Defect formation in metal–organic frameworks initiated by the crystal growth-rate and effect on catalytic performance. *J. Catal.* **2017**, *354*, 84–91. [CrossRef]